Interfacial rheology of model particles at liquid interfaces and its relation to (bicontinuous) Pickering emulsions

J H J Thijssen[1]‡ and J Vermant[2]

[1]SUPA School of Physics and Astronomy, The University of Edinburgh, Peter Guthrie Tait Road, Edinburgh EH9 3FD, UK

[2] Department of Materials, ETH Zürich, Vladimir-Prelog-Weg 5, Zürich CH-8093, Switzerland

E-mail: j.h.j.thijssen@ed.ac.uk

Abstract. Interface-dominated materials are commonly encountered in both science and technology, and typical examples include foams and emulsions. Conventionally stabilised by surfactants, emulsions can also be stabilised by micron-sized particles. These so-called Pickering-Ramsden (PR) emulsions have received substantial interest, as they are model arrested systems, rather ubiquitous in industry and promising templates for advanced materials. The mechanical properties of the particle-laden liquid-liquid interface, probed via interfacial rheology, have been shown to play an important role in the formation and stability of PR emulsions. However, the morphological processes which control the formation of emulsions and foams in mixing devices, such as deformation, break-up, and coalescence, are complex and diverse, making it difficult to identify the precise role of the interfacial rheological properties. Interestingly, the role of interfacial rheology in the stability of *bicontinuous* PR emulsions (bijels) has been virtually unexplored, even though the phase separation process which leads to the formation of these systems is relatively simple and the interfacial deformation processes can be better conceptualised. Hence, the aims of this topical review are twofold. First, we review the existing literature on the interfacial rheology of particle-laden liquid interfaces in rheometrical flows, focussing mainly on model latex suspensions consisting of polystyrene particles carrying sulfate groups, which have been most extensively studied to date. The goal of this part of the review is to identify the generic features of the rheology of such systems. Secondly, we will discuss the relevance of these results to the formation and stability of Pickering-Ramsden emulsions and bijels.

Keywords: Interfacial rheology, Colloidal particles, Liquid interfaces, Pickering, emulsions, foams, bijels, bicontinuous.

‡ Corresponding author: j.h.j.thijssen@ed.ac.uk, https://www.ph.ed.ac.uk/~jthijsse/

1. Introduction

Interface dominated materials are materials with a high fraction of internal surface area, i.e. their total interfacial area is much larger than the area of their container [1]. A well-known example of such a material is an emulsion: a dispersion of droplets of liquid A in an immiscible liquid B [2, 3]. Emulsions are found in many branches of science and technology ranging from food products such as milk, over consumer products such as skin cream, as well as in technological applications such as agricultural sprays, drilling fluids and water-crude oil mixtures [4, 5]. As the energy cost per unit of liquid-liquid contact area (the interfacial tension γ) is finite [6], emulsions tend to phase separate macroscopically to minimize their interfacial energy. Typically, a third component is required to prevent this phase separation. Conventionally, this third component is a surfactant: a molecule with a hydrophilic head group and a hydrophobic tail [7]. Surfactants can stabilize emulsions by accumulating at the liquid-liquid interface, thereby lowering the interfacial tension and providing repulsive interactions between droplets (steric or electrostatic) [8].

In recent decades, there has been a revived interest in emulsions stabilized by micron-sized particles rather than surfactants [9–12]. These so called Pickering-Ramsden (PR) emulsions are interesting for several reasons: they are i) model arrested systems [13], ii) promising templates for advanced materials [14–18], iii) rather ubiquitous in industries ranging from foods to petrochemicals [4, 5] and iv) the stabilizing particles affect surface energy and wetting properties less when compared to surfactants. One crucial difference between surfactants and particles is that the latter can irreversibly attach to liquid interfaces [19, 20]. For a spherical particle at a flat interface, this is quantitatively described by

$$\Delta G = \pi r^2 \gamma \left(1 - |\cos\theta|\right)^2 \ , \tag{1}$$

in which ΔG is the detachment energy per particle [21]. Even for a particle of radius $r = 1$ μm and contact angle $\theta = 75°$ [22] at a water-oil interface of tension $\gamma = 50$ mN $\cdot$ m^{-1} [23], $\Delta G \sim 2 \cdot 10^7$ $k_\mathrm{B}T$ (Boltzmann constant k_B [24] and temperature $T = 25$ °C). Hence, once particles have attached to a liquid interface, they are unlikely to detach under quiescent conditions. Moreover, the trapping energy of a particle at a curved liquid interface depends on the curvature, providing a driving force for particles towards strongly curved regions [25].

Both for production and use, the mechanical properties of PR emulsions are often pivotal [4]. In the case of skin cream, for example, they need to have a bulk yield stress to prevent sagging under gravity, but they need to be liquid-like when spreading it across your skin. The mechanical properties of these high-interface materials strongly depend on the mechanical properties of the interfaces themselves [26–28]. Both surfactant and particle-stabilized emulsions can exhibit elastic, solid-like behaviour, even though they

consist almost entirely of viscous liquids [29, 30]. The quantitative study of the mechanical properties of liquid-fluid interfaces is known as interfacial rheology [31–34]. Much like for bulk materials, interfacial rheology seeks to describe the relations between stresses and deformations by measuring a limited number of material functions in experiments with well-defined kinematics and then using constitutive relations to predict the behaviour in more complex situations.

For bulk materials, the rheology in shear or extensional flow often suffices to describe the material behaviour during usage or processing. Similarly for interfaces, shear and extensional viscosities can be defined and measured [35]. However, interfaces are compressible and can be bent, so the response to changes in area or curvature must also be determined. Dilatational rheology interrogates the changes in area A at constant shape, e.g. by measuring the thermodynamic state variable called 'surface pressure',

$$\Pi\left(A\right) = \gamma_0 - \gamma\left(A\right) \ , \tag{2}$$

which is the interfacial tension of the pristine interface (γ_0) minus the one of the interface covered with material ($\gamma\left(A\right)$). However, ordered colloidal phases can display (visco)elastic behaviour, in which case the measured surface pressure may be an *effective* surface pressure, containing contributions related to the changes in the equilibrium properties as well as the extra and deviatoric stresses [36]. Note that, for some particle monolayers, it is possible to separate the thermodynamic and rheological contributions to the effective surface pressure [37]. It should also be noted that many techniques measure a combination of shear and dilatation [38], for example for the pendant drop technique this was recently shown in detail [39]. Properties related to bending are mainly obtained from the analysis of wrinkled layers [40, 41].

Non-dimensional numbers are useful for determining the relative importance of different effects. The Boussinesq number measures the role of stresses stemming from interfacial rheology relative to bulk fluid mechanics stresses. It will be important during practical applications, but it also provides guidance when performing rheological measurements. For interfacial shear rheology it can be defined as:

$$Bo_{\mathrm{s}} = \frac{\eta_{\mathrm{s}}}{\eta a} \ , \tag{3}$$

where η_{s} is the interfacial viscosity, η is the bulk viscosity of the subphase and a is a dimension related to the measurement set-up [42]. As Bo_{s} is essentially the ratio between interfacial and bulk stresses, Bo_{s} needs to larger than 1, otherwise the interfacial measurement may be dominated by bulk flows [43]. For example, for double-wall ring measurements on polystyrene particles (surface coverage 77%) at an interface between air and water-glycerin (with 0.4 M NaCl) [44]

$$Bo_{\mathrm{s}} = \frac{\eta_{\mathrm{s}}}{\eta a} \sim \frac{0.01 \ \mathrm{Pa \cdot s \cdot m}}{2.5 \cdot 10^{-3} \ \mathrm{Pa \cdot s \cdot 0.001 \ m}} \sim 10^3 \ , \tag{4}$$

showing the feasibility of such measurements [45, 46].

Considering disks on a liquid interface, Elfring *et al.* [47] define a second Boussinesq number for dilational stresses relative to bulk stresses. Following Erk *et al.* [48], who considered flow within liquid droplets, one can similarly define this second Boussinesq as

$$Bo_{\mathrm{d}} = \frac{\kappa_{\mathrm{s}}}{\eta a} \ , \tag{5}$$

in which κ_{s} is the interfacial dilatational viscosity. Alternatively, Verwijlen *et al.* [35, 49] introduce the dimensionless group

$$\Theta = \frac{\kappa_{\mathrm{s}}}{\eta_{\mathrm{s}}} \ , \tag{6}$$

which is the ratio between the interfacial dilatational (κ_{s}) and the interfacial shear viscosity (η_{s}), to complete the description of the interface. For a complex, mixed deformation, an interface will escape the more "expensive" deformation: when Θ is small a dilatational deformation will be easier, with the opposite being true for large values of Θ or $Bo_{\mathrm{d}}/Bo_{\mathrm{s}}$.

A final important non-dimensional number is the Marangoni number. When a homogeneous dilatational deformation takes place, the compressibility of the interface will give rise to an elastic response. However, when this deformation is not homogeneous, additionally the local surface concentration of the surface active species can vary and the local surface tension is altered. This can create restoring Marangoni flows that will try to equilibrate the interfacial concentrations. The Marangoni number characterises both those forces. It is defined as:

$$Ma = \frac{K\Gamma_0}{\eta^{(\mathrm{s})}\dot{\gamma}_{\mathrm{s}}} \ . \tag{7}$$

K is the slope of the (apparent) isotherm at a surface pressure Π, where $\Pi = \gamma_0 - \gamma$ is the surface tension of the pristine interface minus the one of the interface covered with material. Γ_0 is the equilibrium surface concentration at a surface pressure Π. The denominator $\eta^{(\mathrm{s})}\dot{\gamma}_{\mathrm{s}}$ is the magnitude of the surface stresses of rheological origin, here taken for a shear flow at a shear rate $\dot{\gamma}_{\mathrm{s}}$. Three non-dimensional groups will appear in the stress boundary condition for a planar interface undergoing a complex surface deformation, either $Bo_{\mathrm{s}}, Bo_{\mathrm{d}}$ number and Ma, or the combination $Bo_{\mathrm{s}}, \Theta, Ma$ [35, 47, 49]. When the interface is curved, effects of capillarity (captured by a Capillary number) and bending will additionally contribute.

It has clearly been established that interfacial rheological properties can play an important role in Pickering stabilisation [50, 51]. For example, enhanced stability of PR emulsions/foams has been linked to maxima in yield and/or melting strains [52, 53]. The idea is that the strength of the interfacial-particle assembly is enough to prevent coalescence upon droplet collisions (even under shear). However, the exact nature of the relationship is not completely clear yet [54]. Recently, Van Hooghten *et al.* [55] have recently pointed out that there may well be a crucial difference between PR emulsions in

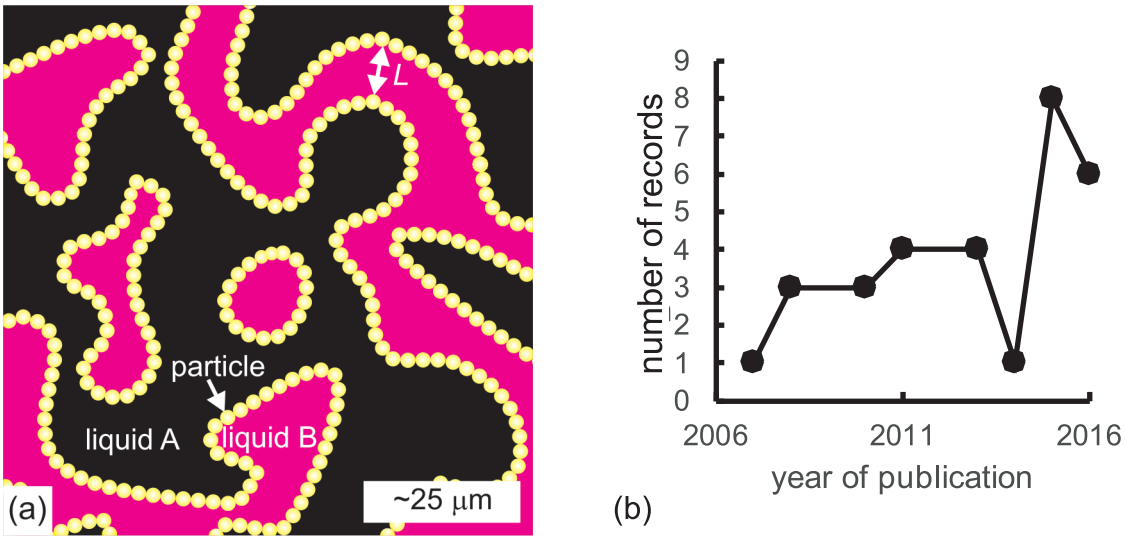

Figure 1. (a) Schematic of a 2D slice through a 3D bijel. (b) Number of records versus pubication year from Web of Science (topic = "bijel OR (bicontinuous Pickering emulsion)") [71]. Note that it seems that the term "bijel" may not have fully established itself yet as a search keyword [58]. Panel (a) from Reeves *et al.* [72].

which interfacial shear rheology dominates versus those in which dilatational rheology dominates; the former are believed to require particles that aggregate in the bulk or at the interface [56, 57], whereas the latter have been shown to be stable in absence of aggregation [30, 55]. Such observations agree that in terms of the stress boundary condition for a planar interface, several properties need to be engineered. Moreover, the morphological processes which control the formation of emulsions and foams in mixing devices include deformation and stretching, droplet or bubble break-up, and (limited) coalescence. Coupled to adsorption processes, this makes it difficult to identify the precise role of the interfacial rheological properties in such systems.

The relationship between interfacial rheology and the stability of *bicontinuous* Pickering emulsions (bijels) has only received limited attention so far [58] . A bijel consists of two tortuous, interpenetrating liquid channels stabilized by a layer of colloidal particles at the liquid-liquid interface (figure 1(a)) [59–61]. This class of materials was predicted by simulation in 2005 [62], first realized in the lab in 2007 [63] and first used for materials synthesis in 2010 [64]. They are typically fabricated by halting spinodal demixing of a binary fluid due to jamming of the colloidal particles at the interface, though other fabrication routes have now been explored [65–67]. The spinodal route requires a binary fluid with a relatively symmetric phase diagram, to ensure roughly equal phase volumes upon demixing, and a contact angle close to 90°; otherwise discrete droplets form instead of continuous channels [68–70].

Bijels have received increasing interest in recent years (figure 1(b)), in no small part because of their potential for application in microfluidics [73], catalyst supports [74], tissue engineering [75] and energy materials [15]. As their characteristic lengthscale, the channel width L (figure 1(a)), and thereby their rheology [59], is tunable between 1 and 500 μm [70, 76], the bulk rheology of bijels has been investigated [77–80]. However, their interfacial rheology has received far less attention, even though bijel formation and stability may well rely on the interfacial rheology of the particle-laden liquid-liquid interface. Moreover, the spinodal route is conceptually appealing to reflect upon the role of the interfacial rheological properties, as the interface is formed in situ and grows and dilates, followed by compression, shear and possibly bending contributions as the interface coarsens and changes shape.

When considering the effect of interfacial rheology on the stability of (bicontinuous) PR emulsions, the presence of the particles at the liquid interfaces leads to a complex response of the interface, with contributions from changes in surface tension (compressibility), responses to shear and dilation as well as potentially bending. This complex mechanical response arises because of particle-particle and particle-interface interactions [77, 81–83], both of which depend on the surface chemistry of the particles used [84, 85]. This makes it difficult to compare results from interfacial-rheology measurements made on liquid interfaces laden with different types of natural [86–91] and/or synthetic [11, 13, 92, 93] particles, especially if they are only accompanied by a limited characterization of the particles themselves. Focussing instead on one type of particle may well simplify the comparison, bringing generic physical principles to the forefront. Fortunately, there are quite a few papers in the literature that have all used the same type of particle: polystyrene spheres made by surfactant-free polymerization, stabilized by sulfate surface groups and typically all obtained from the same producer (IDC). As these suspensions have also been extensively characterized [22, 94–100], they are our choice of model particles for elucidating the typical features of the rheology of particle-laden interfaces in this review.

Given the above, this review aims to 1) evaluate the literature on the interfacial rheology of colloidal monolayers, with a strong focus on the most studied systems, those of charged polystyrene particles at oil-water interfaces, and 2) discuss the outstanding issues relevant to the stability/formation of (bicontinuous) Pickering emulsions. We start by describing in more detail the model particles considered in this review (IDC polystyrene-sulfate) in section 2. In section 3, we continue by reviewing the relevant interfacial-rheology literature, for our choice of model particles. This section has been split into four parts: (3.1) Langmuir-trough results, (3.2) pendant-drop results, (3.3) shear-rheology results and (3.4) bending-stiffness results. Following that, in section 4, we consider the role of interfacial rheology in stabilizing Pickering emulsions (section 4.1) and bijels (section 4.2). We conclude with a summary and an outlook on interesting paths for future research in Section 5.

Table 1. Typical values for some physical quantities for IDC polystyrene-sulfate spheres [22, 94, 95, 98–101]; r is particle radius.

Property	Reported value	Notes
Mass density	1.055 g · cm^{-3}	
Deformability	rigid	
Dielectric constant	2.49-2.55	at 1 kHz flat to 1 GHz
Refractive index	1.59	at 590 nm
Glass transition temperature	100-110 °C	T_g
Sign of charge	negative	at least for pH 4 to 9
		at least for 10^{-6} to 10^{-2} M monovalent salt
Contact angle	73 to 74°	for $r = 2.0$ to 4.8 μm at water-air
	101 to 116°	for $r = 0.05$ to 4.8 μm at water-decane

2. Model particles: charged PS latex spheres

Before reviewing the interfacial rheology of model particle suspensions at liquid interfaces, we first review the basic information regarding the particles of choice [94]; additional characterization is available in the literature [22, 95–100]. Typical values for some physical quantities for polystyrene-sulfate particles are listed in Table 1 [94].

The latex beads we focus on here are polystyrene spheres in the colloidal size range. This means that, intrinsically, the surface of these beads is hydrophobic, which typically results in strong (physical) adsorption of surfactant molecules (if added). As these particles are made by surfactant-free emulsion polymerization, the ends of the polymer chains sticking out usually consist of charged groups, which can provide charge stabilization versus colloidal aggregation. This is an important consideration, because it means that the particles do not require surfactants to be stable, substantially alleviating the interpretation of interfacial experiments. Typical examples of surface groups include: amidine, amine and carboxylate; here we focus on sulfate-terminated polystyrene spheres.

IDC's sulfate-terminated polystyrene spheres, from now on referred to as "PS-S", cover the entire colloidal size range, i.e. from 0.02 μm to 10 μm [94]. The manufacturer provides sizes obtained by imaging at least 500 particles in transmission electron microscopy (TEM), calibrated using a diffraction grating replica. The quoted size is a number average diameter (D) and the polydispersity or coefficient of variation (cv) is the standard deviation expressed as a percentage of D. It is worthwhile noting here that the (hydrodynamic) radius of IDC PS-S particles in solution is larger than the TEM size provided by the supplier, as reported by several papers using e.g. hydrodynamic fingerprinting [95], dynamic light scattering [96] and photon correlation spectroscopy [98, 99]. As polystyrene colloids can shrink 1) upon removal of the solvent [102], 2) upon expo-

sure to an electron beam [103] and/or swell in certain solvents [104], it is perhaps no surprise that the in-situ size of IDC PS-S particles is larger than their dry (TEM) one.

Given their size ($\leq$ 10 μm) and density ($\rho_{\mathrm{PS-S}} \sim \rho_{\mathrm{water}}$), it is unlikely that these spheres cause liquid-interfacial deformation due to gravity [105], which would in turn lead to capillary attractions between the spheres. However, when considering an interfacial experiment, it is generally a good idea to calculate the corresponding Bond number

$$N_{\mathrm{b}} = \left(\frac{r}{l_{\mathrm{c}}}\right)^2 \ , \tag{8}$$

in which r is the particle radius and $l_{\mathrm{c}} = \sqrt{\gamma/\rho_{\mathrm{l}} g}$ (liquid density ρ_{l} and acceleration of gravity g) [106]. Even for a particle with a radius of 10 μm, $N_{\mathrm{b}} \sim 2 \cdot 10^{-5} << 1$, so flotation capillary forces are unlikely to be significant [105].

Regarding surface-charge density, about 5 to 10% of the PS-S surface is occupied by sulfate groups. The manufacturer determines the surface charge of their microspheres using titration. The surface charge density σ is calculated as

$$\sigma = \frac{E_{\mathrm{t}}}{\mathrm{SSA}} F \ , \tag{9}$$

where F is the Faraday constant, $\mathrm{SSA} = 6/\left(D\rho_{\mathrm{p}}\right)$ is the specific surface area, ρ_{p} is the particle mass density and E_{t} is the equivalence point of the titration (determined conductometrically) [94]. Typical values of surface-charge density are between 1 and 10 $\mu\mathrm{C} \cdot \mathrm{cm}^{-2}$. It should be noted here that Feick and Velegol have found 50-75% variations versus the average zeta-potential for 4.3 μm IDC PS-S particles [100]. They suggest that the substantial charge non-uniformity on the surfaces of these colloids could be due to the synthesis procedure: primary particles coagulating during surfactant-free emulsion polymerization [107], which could lead to charge non-uniformity if the primary particles have different numbers of charged groups on their surface and substantial heterogeneity. This does align with direct measurements of the interaction forces between these particles at oil-water interface, which exhibit a distribution of magnitudes in which the force depends on the particle pairs tested and sample preparation method [108]. Another possibility suggested by Feick and Velegol is that sulfate groups can be reduced to hydroxyl groups with age [100, 107]. Note that, given the suggested origins, both of these are likely to be nonidealities common to many colloidal dispersions i.e. not just specific to IDC PS-S particles.

From equation (1), it can be seen that the particle-liquid-liquid contact θ is an important parameter, as it co-determines the particle detachment energy. The contact angle of IDC PS-S particles at water-alkane interfaces has previously been measured. For example, Paunov measured the contact angle of PS-S particles at liquid interfaces using a gel-trapping technique, in which the aqueous phase is gelled [22]. The particle is trapped in the gel and the contact angle can be determined via inspection using

electron microscopy or atomic-force microscopy. For PS-S particles at a water-decane interface, Paunov found $(111 \pm 4)^\circ$ for 9.6 μm diameter particles and $(101 \pm 3)^\circ$ for 3.9 μm diameter particles. Slightly higher values of about 130° were obtained by Reynaert *et al.* [109] for 3.1 μm diameter particles, and these values were shown to be essentially independent of electrolyte concentration. Isa *et al.* [101] compared this to freeze-fracture shadow-casting electron microscopy (FreSCa), in which the cryo-frozen sample is fractured along the interface and the contact angle is determined from the shadow cast by the particle under oblique illumination by the electron beam. For 2.8 μm diameter PS-S particles at a water-decane interface, they found $(85.0 \pm 5.2)^\circ$ using FreSCa and $(122.0 \pm 4.1)^\circ$ using AFM gel trapping.

These results suggest that the reported contact angle of PS-S particles at water-oil interfaces may vary with measurement technique and particle size (the latter presumably due to differences in surface chemistry and/or charge). The contact angle was also shown to be a decreasing function of the aspect ratio when spherical PS particles are stretched into ellipsoids [110]. Despite the very large interfacial energy gradient driving the adsorption, the equilibrium may be reached only very slowly after particles breach the liquid-liquid interface [111, 112]. As there is always the risk that gelling affects the contact angle before it is measured, we suggest measuring the contact angle of PS-S particle at water-oil interfaces using an in-situ technique like transmittance measurements [113] or the usage of FreSCa [101] while carefully controlling the equilibration times.

3. Interfacial rheology of model particle suspensions at liquid interfaces

Particle laden interfaces are prime examples of structured, complex fluid interfaces with an interfacial microstructure, and they exhibit interfacial rheological properties which can be described by material functions. A wide range of techniques has been used to probe the structure-property relations in particle monolayers. Results obtained using a Langmuir trough, a pendant drop, a magnetic needle surface rheometer and a double-wall ring will be discussed and compared to results of simulations.

In a typical Langmuir trough, two straight barriers are used to change the area of a rectangular area of liquid interface while measuring the apparent interfacial tension γ_p using a Wilhelmy plate (figure 2(a)) [28, 114]. In pendant-drop tensiometry, a drop is produced using a needle and the area of the drop is changed by changing the volume of the drop (figure 2(b)). For simple interfaces the interfacial tension is obtained by fitting the Laplace equation to the extracted drop profile i.e. assuming that the droplet shape is a balance between gravity and interfacial tension [115]. For more intricately structured interfaces, drop shape analysis needs to be extended to determine the material parameters which characterise the elasticity [41] or the stresses and strains have to be obtained directly from local force balances [39].

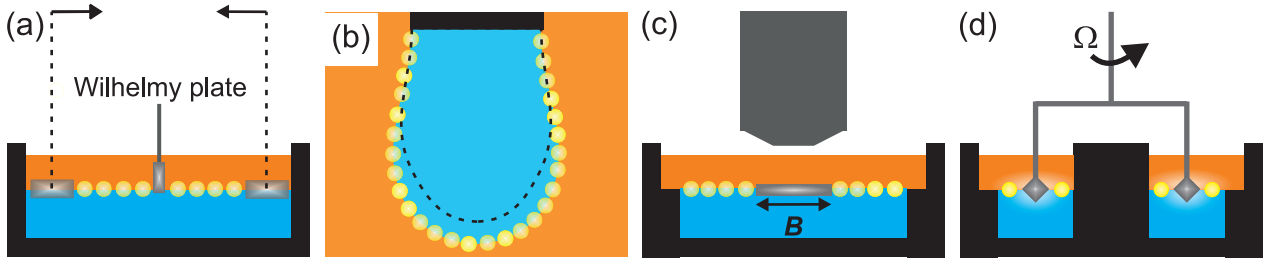

Figure 2. Schematics for the measurement techniques corresponding to results presented here: (a) Langmuir trough, (b) pendant drop, (c) magnetic needle surface rheometer and (d) double-wall ring. Panel (d) adapted from Ref. [55].

In dilatational measurements, the effects of compressibility intermix with the mechanical response and few measurements are truly simple dilatational deformations [36, 38, 39]. Shear rheometry is more straightforward. In a magnetic needle surface rheometer, magnetic fields are used to exert a known shear stress onto a magnetic needle that is floating at the liquid interface and the resulting deformation is monitored using a microscope (figure 2(c)). The double-wall ring is the interfacial equivalent of a double wall Couette cell; a ring is attached to a stress-controlled, rotational rheometer and positioned in the liquid interface (figure 2(d)). For further details, we refer the reader to existing reviews on interfacial-rheology measurement techniques [32–34, 116, 117].

3.1. Langmuir trough

Langmuir-trough measurements (figure 2(a)) provide insight into how (effective) surface pressure Π, i.e. the resistance of the particle monolayer to further compression, varies with changes in surface coverage on a flat liquid interface. This is particularly relevant to bijels, as their area-averaged mean curvature $\langle H \rangle = 0$ [64, 118]. In short, the surface coverage of particles increases during phase separation, which is expected to halt as and when the effective surface pressure reaches a value equal to the liquid-liquid interfacial tension (section 4.2). This is also an important consideration for Pickering emulsions ($\langle H \rangle > 0$), as the apparent interfacial tension is 0 when $\Pi = \gamma$, which means the driving force for further coarsening via coalescence and Ostwald ripening vanishes [8].

Aveyard *et al.* [119] were the first to study the structure and collapse of monolayers of PS-S particles (from IDC) at water-air and water-oil interfaces using Langmuir-trough isotherms and direct microscopic observations. They used particles with a range of diameters d and surface-charge densities σ (see Table 1 in [119]), but focussed on $d = 2.6$ μm, $\sigma = 7.7$ $\mu\text{C} \cdot \text{cm}^{-2}$ and contact angles at the water-oil interface of 70° to 80°. Above the collapse surface pressure of 48 $\text{mN} \cdot \text{m}^{-1}$, Aveyard *et al.* found that the particle-laden interfaces buckle and wrinkle (figure 3(a)), but no expulsion of individual particles or particle aggregates from the liquid interface was observed. The wrinkles were oriented

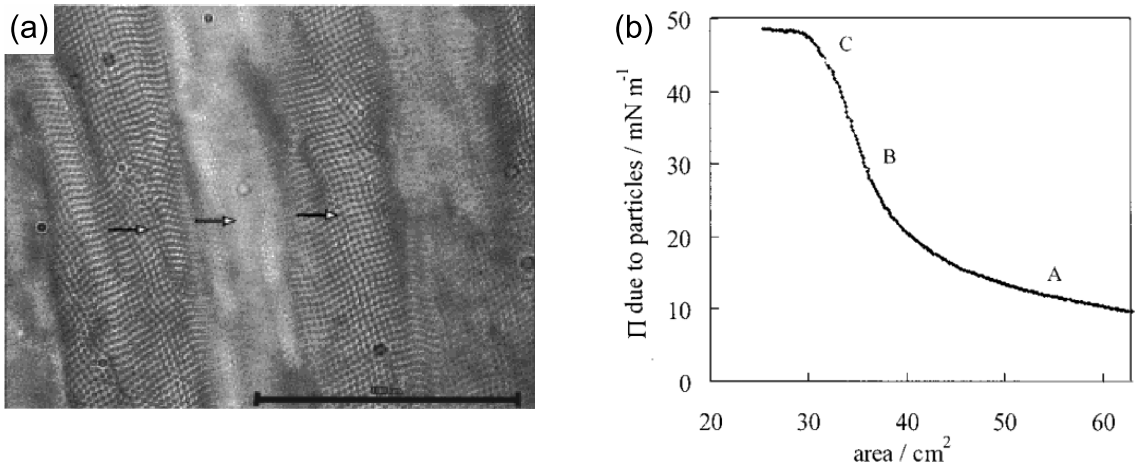

Figure 3. (a) Collapsed monolayer of 2.6 μm diameter polystyrene particles at the water-octane interface far above the collapse pressure. Large wrinkles have appeared, parallel to the barriers of the Langmuir through, but neither individual particles nor rafts of particles are expelled from the monolayer. Scale bar represents 100 μm. (b) Surface pressure-area isotherm for 2.6 μm diameter polystyrene particles at the water-octane interface. The surface pressure (2 mN/m) due to the spreading solvent has been subtracted from the ordinate. The various letters are referred to in the text. Both panels adapted from Ref. [119].

perpendicular to the compression direction, had a wavelength of about 100 μm and an amplitude of about 20 μm. Upon re-expansion of the monolayer, mainly individual particles but also some aggregates were observed, suggesting that compression and expansion is more or less, but not completely reversible. Particles are, however, typically not expelled.

The corresponding isotherms, recorded using filter-paper Wilhelmy plates, show three distinct regions (figure 3(b)). At high areas, the surface pressure Π rises relatively slowly (region A), which the authors attribute to long-range (soft) repulsions between the interfacial particles. As the area is reduced on compression, Π begins to rise more steeply (region B) until ultimately the rate of Π increase begins to fall; the locus of the rapid change in slope (C) is identified as the collapse pressure of the monolayer and is sometimes referred to as a "knee". As the particle monolayers remain highly ordered even when using concentrated electrolyte solutions for the aqueous phase, Aveyard *et al.* [120] attribute the long-range repulsion between the latex particles at the water-oil interface to electrostatic interactions, through the oil phase, of residual charges residing at the particle-oil interface. Quantitatively comparing their measurements to a theoretical model, which includes the usual Coloumbic force and the image force due to the existence of the oil-water surface, they obtain a percentage surface ionization of sulfate

groups at the particle-oil interface of about 10^{-2} [119], although in another paper they report values as low as $3 \cdot 10^{-4}$ [120].

Comparison with simulations was provided by Sun and Stirner [121], who used molecular dynamics simulations to calculate surface pressure-area isotherms for the compression of monolayers consisting of charge-stabilized polystyrene particles at the oil-water interface. They also compare their results to the experiments by Aveyard *et al.* [119], mainly in an attempt to elucidate the interparticle interactions. First of all, they show that the finite particle size must be taken into account to accurately describe interparticle interactions for separations smaller than $3\times$ the particle radius (figure 4(a)). Their results indicate that at low coverage only charge-charge interactions are sufficient to describe the experimentally observed pressure-area isotherms. For high surface coverage, however, the experimental data is described well by calculations that assume dipole-dipole interactions only (figure 4(b)). Comparing simulated and measured isotherms yields values for surface charge density and dipole moment that are both consistent with traces of water trapped at the oil-particle interface, with a dissociation ratio of the order of 10^{-2}. It is unclear what would control the number of charges on the oil side and the variability of reported values of the charge dissociation is worrysome. Recent reports suggests that the rubbing between the particles and oil leads to the spontaneous accumulation of negative charges on the hemisphere of those interfacial particles that contact the oil phase by means of triboelectrification [122] which subsequently relax. This would imply that the results will vary on how the monolayers are produced and equilibrated.

However, it should also be noted that detailed measurements of the dependence on electrolyte concentration of the equilibrium force using optical tweezers reveal a weak, but a clearly non-negligible dependence on the Debye length $\kappa^{-0.43}$, which seems to be at odds with the oil-side charges dominating the interaction [123]. Also when salt is added to the aqueous subphase, aggregation can be readily induced [109] in layers which have been equilibrated for a long time. Detailed measurements of the interaction using an array of techniques show that the magnitude of the dipolar force and the relative changes as a function of electrolyte concentration measured using tweezers were in quantitative agreement with predictions taking only water-side charges into account. Yet, detailed calculations using the Langevin Poisson-Boltzmann equation were required, and the usual simplifications of neglecting the finite ion size and the detailed polarization saturation of the medium were not made [124–126]. Hence, oil-side charges need not be invoked to explain the observed magnitude and details of electrolyte dependence for layers at equilibrium.

Furthermore, the water-side charges cannot be ignored when discussing the overall interaction and they also lead to strong dipolar interactions. How oil-side and water-side effects contribute to the overall interaction remains an open question. However, it

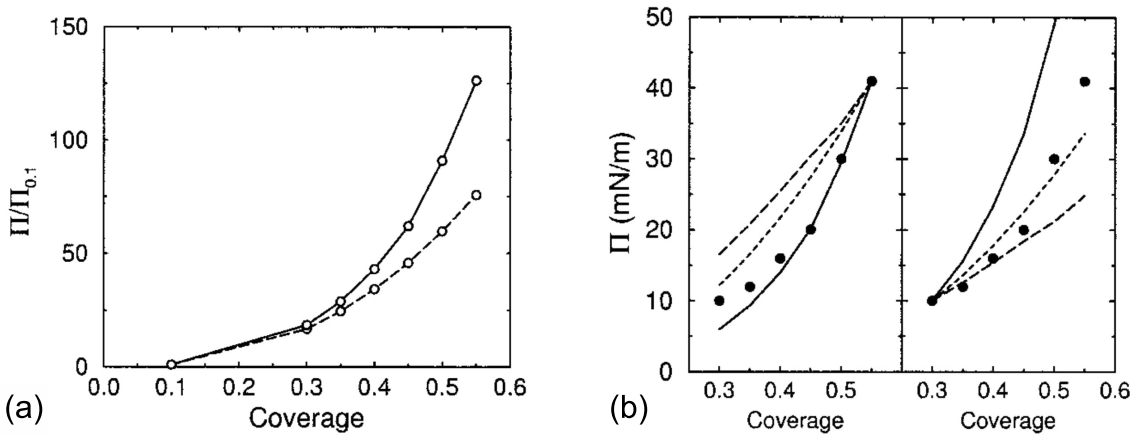

Figure 4. (a) Calculated surface pressure Π (normalized to Π at coverage 0.1) versus coverage for a monolayer of (dashed) point particles and (full) particles of diameter 2.6 μm under dipole-dipole interactions. (b) Calculated surface pressure versus coverage for a monolayer of 2.6 μm diameter particles under (dashed) charge-charge, (dotted) charge-dipole and (full) dipole-dipole interactions. (circles) Experimental data taken from Ref. [119]. Both panels adapted from Ref. [121].

is clear that electrostatics at oil-water interfaces are strong, with dipolar contributions and unusual effects of electrolyte concentration, counterion sizes, spreading protocols and possibly triboelectrification. These electrostatic phenomena may enhance emulsion stability, especially for oil-continuous emulsions due to the lack of screening. How important these electrostatic interactions are in bijels from binary liquids is not clear, for example triboelectric effects are not very likely for the oil-side charges and, moreover, any trapped aqueous phase would dissolve rapidly due to partial miscibility, i.e. bijel channels are not 'water' and 'oil' but water-rich and oil-rich. For example, in the case of water-lutidine/silica bijels, the lutidine-rich phase still contains 9 wt-% water at 45 °C and so interparticle interactions are unlikely to be completely unscreened in either phase.

Aveyard *et al.* [127] used a similar system (IDC PS-S of diameter $d = 2.6$ μm and surface-charge density $\sigma = 7.7$ $\mu\mathrm{C} \cdot \mathrm{cm}^{-2}$ at water-octane) to investigate whether the buckling transition occurs when the interparticle forces per unit length in the interface are equal to the surface tension of the liquid-liquid interface (see figure 5(a)); the latter was varied by adding anionic (SDS), non-ionic (DBG) and cationic surfactants (CTAB, CPC). They also develop a model for the buckling transition that assumes a fixed contact angle for the particles at the water-oil interface, i.e. it does not allow particles to be expelled from the interface, but it does allow the formation of corrugations of amplitude e [127]. Denoting the Langmuir-trough area at the onset of collapse as

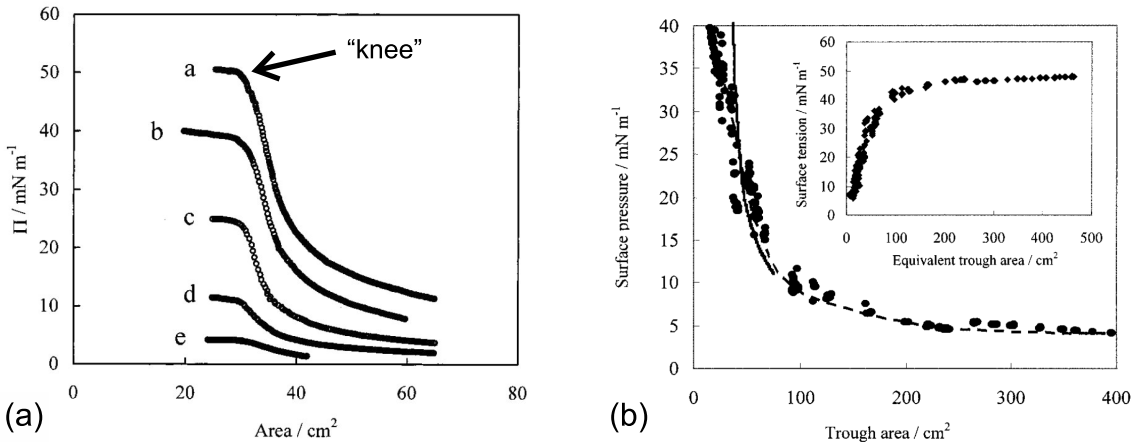

Figure 5. (a) Surface pressure-area isotherms for 2.6 μm diameter polystyrene particles (IDC) at the octane-aqueous solution interface: (a) no surfactant, (b) 0.1 mM SDS, (c) 0.1 mM DBG, (d) 0.5 mM DBG and (e) 1 mM CTAB. The arrow indicates what is referred to in the text as a "knee". (b) Apparent surface pressure measurements on the same system without surfactant (pendant drop: filled symbols and dashed lines; Langmuir trough: full line; drop areas converted to equivalent Langmuir-trough areas). Both panels adapted from Ref. [127].

A_{L}, the model predicts that the liquid-interfacial area $A\,(e)$ and free energy are both constant as a function of the in-plane area between the barriers A_0 for $A_0 < A_{\mathrm{L}}$. In this regime, as A_0 is decreased, $A\,(e) = A_{\mathrm{L}}$, maintaining a balance between interparticle and surface-tension forces. As a result, the surface pressure Π is constant and equal to the liquid-liquid surface tension γ, which aligns with their observations.

It should be emphasized that the buckling analysis *assumes* that particles are not expelled from the Langmuir-trough interface and, hence, it does as yet not *explain* why this does not happen, nor why they can be expelled from a pendant drop [128]. As the surface fraction $\phi < 1$, removing a particle from the interface and allowing the interface to contract to restore the value of ϕ is always energetically favourable, i.e. the particle cross-section is always smaller than the contracted liquid-liquid contact area. However, there is an energy barrier for particle expulsion: particles can only be expelled in 'units' of their detachment energy per particle (equation (1)). In contrast, there is no energy barrier to buckling, i.e. the amplitude e can change continuously as the in-plane area A_0 is reduced, which may well explain why buckling rather than expulsion is observed in (initially flat) particle monolayers at liquid interfaces.

In Ref. [127], Aveyard *et al.* qualitatively compare their experimental results to simulations of nanoparticles by Fenwick *et al.* [129], which display a collapse mode via

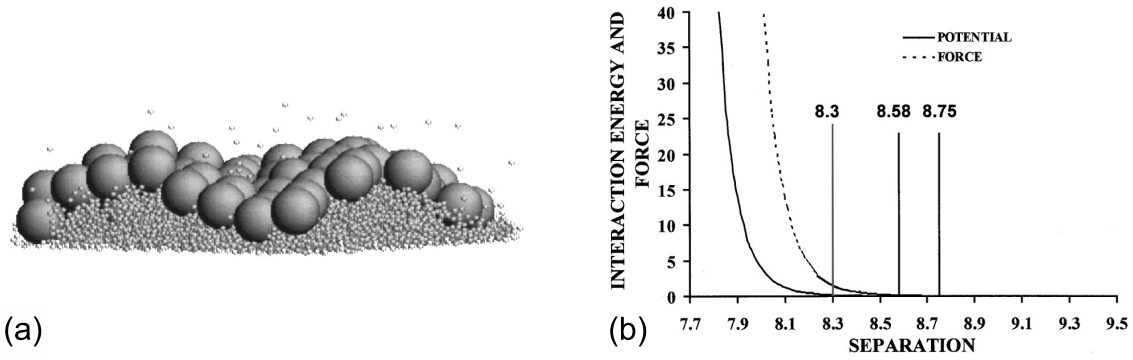

Figure 6. (a) Simulation snapshot of a compressed monolayer of particles (grey) at a liquid-vapor interface. The liquid/vapor molecules are the white spheres of diameter $\sigma_{\rm f}$ and the particle diameter $\sigma_{\rm p} = 8\sigma_{\rm f}$. Note that both the close-packed monolayer and the liquid-vapor interface are corrugated. (b) Interparticle interaction force and energy (in simulation units of $\epsilon = 0.5\ k_{\rm B}T$) versus interparticle separation (in units of $\sigma_{\rm f}$). The vertical full lines represent estimates of particle diameters from the simulated pressure-area isotherm, using three methods often employed with experimentally determined isotherms (see text for details). Both panels adapted from Ref. [129].

buckling similar to the one observed in experiments. Fenwick *et al.* report molecular dynamics simulations of a system of 64 particles at a liquid-vapour interface. The particles have a diameter $\sigma_{\rm p} = 8\sigma_{\rm f}$, where $\sigma_{\rm f}$ is the diameter of a solvent particle (so if the solvent is water then the particle is $\sim$ 1 nm) and contact angle $\theta = 100°$; the interparticle interaction is described as a purely repulsive Lennard-Jones potential. As in experiments, the simulated surface pressure was determined using

$$\Pi\left(A\right) = \gamma_{\rm s} - \gamma\left(A\right) \ , \tag{10}$$

where γ_s is the surface pressure of the solvent and $\gamma\left(A\right)$ is the apparent surface tension of the monolayer interface, both calculated from the simulation data in this case. The calculated pressure-area isotherms show features also observed in experiments, especially a "knee" below which surface pressure and interfacial tension are constant and equal (Fig. 5(a)). Simulation snapshots confirm that this knee is the onset of particle monolayer collapse via buckling (figure 6(a)). It is worth pointing out here that the interparticle force extracted from the simulated pressure-area isotherm is larger than the bare (input) interaction force (by about a factor of 4), which the authors ascribe to the presence of the solvent molecules [130]. However, as mentioned above, the (visco)elastic response of ordered monolayers under compression in a Langmuir trough can interfere with surface-pressure/area isotherm measurements, in particular as the compression experiments are carried out at finite speeds and significant deviatoric stresses are possibly introduced where both the area and shape are changed [36, 37].

Fenwick *et al* also compare their simulations to two theoretical models: particle

promotion (i.e. particles changing their contact angle by shifting perpendicularly to the liquid-vapour interface) and buckling (figure 6(a)). In particular, particle promotion is described as one third of particles staying put, one third moving into the liquid phase and one third moving into the vapour phase, effectively forming a tri-layer of particles. Note that this decreases the average in-plane interparticle distance and is hence one way for the system to cope with a trough area smaller than the area required for a (flat) particle monolayer. In this model, surface pressure at the collapse area is $1.21\times$ the liquid-vapour surface tension γ_{lv}, leading to a negative apparent surface tension of the interface containing the particles. The second model considers buckling of the interface, i.e. all particles keep the same contact angle and the liquid-vapour contact area is constant once close packing has been reached (even though the trough area can still decrease). In this model, surface pressure is $1 < 1.21\times$ the liquid-vapour surface tension. Assuming a quadratic potential and a triangular corrugation, this model shows very good agreement with the simulated isotherm, especially near the critical surface pressure (and the simulated isotherm qualitatively resembles experimental data [127]). Comparing the two models indeed implies that buckling rather than ejection should be observed when compressing a particle monolayer, as particle promotion is a necessary requirement of ejection and the interface can buckle at surface pressures below those required for particle promotion. Note that this aligns with the conclusion that there is an energy barrier to particle ejection, which should not exist for monolayer buckling.

Fenwick *et al.* make some important points about the experimental characterization of interparticle forces from Langmuir-trough data and how it crucially relies on the correct interpretation of certain features therein. They also claim this is not always correctly done, partly because of the complex behaviour observed in particle monolayers upon compression (fracture, buckling or loss of material). One particular concern is that pressure-area isotherms are often converted to pressure-coverage isotherms. This step requires knowledge of particle surface coverage, which is often extracted from experimental isotherms in one of three ways:

(i) A tangent is drawn to the linear part of the isotherm at surface coverages just below close packing and the intercept with the horizontal axis is taken to be the close packing area.

(ii) The "knee", i.e. where the critical surface pressure is reached, is used to determine the close packing area; often via the intercept of the tangent drawn in method (1) and the tangent to the (nearly) horizontal part at low area.

(iii) The experimental data are fitted to the ideal 2D gas law, $\Pi A = \Pi A_{\mathrm{hcp}} + k_{\mathrm{B}}T$, in which A is the interfacial area per particle and A_{hcp} is the estimated close-packing area per particle [131].

To demonstrate their concern, the authors employ all three methods to their simulated pressure-area isotherm, leading to three quite different particle diameters: $8.75\sigma_{\mathrm{f}}$, $8.30\sigma_{\mathrm{f}}$ and $8.58\sigma_{\mathrm{f}}$, respectively. Method (1) is only valid if the steep rise just before the

knee is almost vertical (i.e. if the interparticle potential is hard), which is not always the case. Method (3) is based on the ideal gas law and therefore cannot be expected to work flawlessly at high particle concentrations (e.g. near close-packing). Given the simulation results by Fenwick *et al.*, method (2) seems most appropriate, though even that is off by nearly 4% compared to the value of $8\sigma_\mathrm{f}$ as defined in the interparticle potential (see figure 6(b))). Hence, care must be taken with calibrating particle surface coverage from features in pressure-area isotherms. In the case of (fluorescent) micron-sized particles, experimental Langmuir-trough data should be complemented with representative micrographs to provide a proper mapping between trough area and surface coverage.

In short, the review of Langmuir-trough data for PS-S particles at liquid interfaces has established that colloidal particles are unlikely to be ejected from a (flat) liquid interface upon monolayer compression; how this links to PE/bijel stability will be discussed in Sec. 4. In terms of the interactions between interfacial particles, though it is clear that electrostatics at oil-water interfaces are strong, it remains an open question how oil-side and water-side effects contribute to the overall interaction, or how this may vary from one system to another and how it may depend on the preparation protocol. These electrostatic interactions can enhance PE stability, but are probably not so relevant to bijel formation, because the partial miscibility of the phases means that 1) any patches of trapped phase would quickly dissolve and 2) any remaining electrostatic interactions would still be screened. Finally, we argue that care must be taken when calibrating particle surface coverage from features in surface pressure-area isotherms and, where possible, surface coverage should be calibrated using alternative methods (e.g. microscopy).

3.2. Pendant drop

Pendant-drop measurements (figure 2(b)) can be used to generate data similar to Langmuir-trough measurements, i.e. how surface pressure Π varies with surface coverage, but on a curved rather than a flat liquid interface. This is particularly relevant to Pickering emulsions, as both pendant and emulsion droplets have finite curvature ($\langle H \rangle > 0$). This can lead to qualitatively different behaviour, for example particles detaching from liquid interfaces via the 'keystone mechanism' (see below and section 4.2) [132]. However, it may also have a bearing on bijels, as they only have an area-averaged mean curvature $\langle H \rangle$ close or equal to 0 [64, 118], i.e. they are not minimal surfaces with $H = 0$ for each point on the interface. However, one disadvantage of pendant-drop versus Langmuir-trough measurements is that, even for small Bond numbers, gravity can strongly affect pendant-drop measurements by creating non-uniform surface coverages.

There are relatively few papers reporting surface pressure-area isotherms measured using a pendant drop, especially for IDC PS-S particles, most likely as it is not easy to

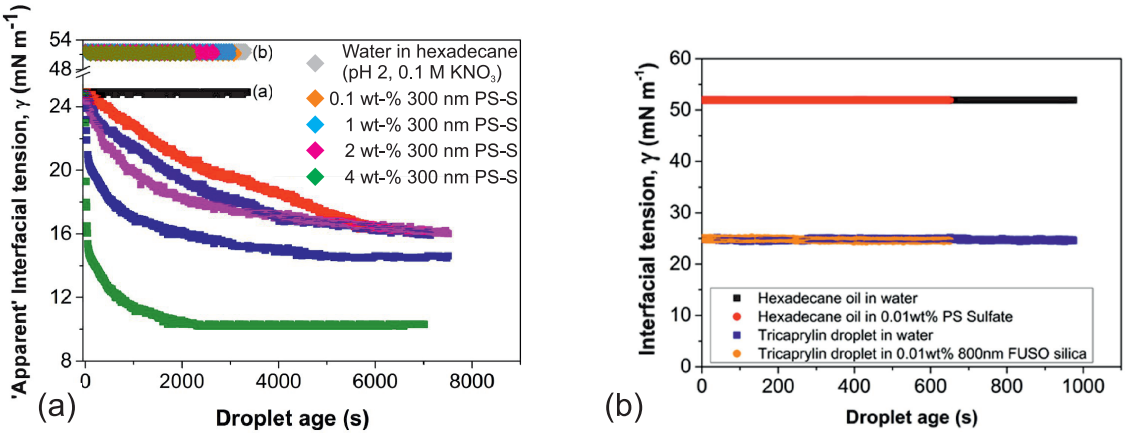

Figure 7. (a) "Apparent" interfacial tension measured using pendant-droplet tensiometry of a water droplet (pH 2, 0.1 M KNO_3), with and without 300 nm IDC PS-S particles, immersed in *n*-hexadecane oil (labelled with "(b)" in this panel). (b) Interfacial tension, measured using microtensiometry, of an *n*-hexadecane droplet (radius 40 μm) in pH 2, 0.1 M KNO_3 water containing a dispersion 0.01 wt-% 300 nm IDC PS-S particles. Both panels adapted from Ref. [133].

generate such droplets with controlled surface coverage. In [127], Aveyard *et al.* compare their Langmuir-trough measurements to pendant-drop measurements and find the two methods to be in agreement, at least at surfaces pressures below 30 $\mathrm{mN \cdot m^{-1}}$. Above this threshold, the surface pressure-area isotherm obtained using the drop method is slightly to the left (lower area) of the one obtained using a Langmuir trough (see figure 5(b)). The authors appreciate that the Laplace equation, used in the analysis of the drop profile to extract tension, may not apply to the potentially rigid interfaces formed at high surface pressures [37]; for a discussion of elastic effects on pendant-drop analysis, see the recent review by Nagel *et al.* [39]. Alternatively, they suggest that particles may be lost from the drop surface as it is retracted, which would mean that curvature plays a decisive role in the behaviour of particles at liquid interfaces i.e. no such particle expulsion was observed at flat interfaces.

Manga *et al.* [133] report pendant-drop and microtensiometry measurements for 300 nm IDC PS-S particles at a water-oil(hexadecane) interface. They show that the apparent interfacial tension (including possibly mechanical contributions) does not change, i.e. is the same as for bare water-oil, upon the addition of 0.1 to 4 wt-% of IDC PS-S particles to the water droplet (see figure 7). They do observe a decrease in apparent interfacial tension upon the addition of silica particles, which they attribute to the "added weight of the particle bed forming at the bottom of the droplet rather than any 'real'

dynamic interfacial tension change". Note that 1) this refers to excess (non-interfacial) particles and 2) this effect is indeed expected to be less pronounced for polystyrene particles, because their density is close to that of water and so they are close to neutral buoyancy. Interestingly, the authors note that the particles had to be thoroughly cleaned, via typically 8 to 10 centrifugation and redispersion cycles, before the supernatant matched the air-water surface tension. Yet, it is likely that the authors have not probed the regime most relevant for bijel formation, i.e. that of (nearly) close-packed interfacial particles where also interfacial viscoelastic stresses may start to contribute. As suggested above, upon close packing, the droplet shape is no longer just a balance between gravity and interfacial tension, so the apparent interfacial tension is expected to differ from the bare water-oil one for close packing. However, the authors do not report changing the area of the droplet in the main text or SI and, given that these are charged particles dispersed in the aqueous phase, it is unlikely that a close-packed layer would form by adsorption without compression.

As in the case of Langmuir-trough measurements, comparing to simulations can help to clarify several experimental results. Gu and Botto reported static and transient 3D molecular dynamics simulations of pendant droplets covered with a monolayer of colloidal particles (figure 8(a)) [134]. They used a purely repulsive interparticle interaction, i.e. a screened Coulombic potential with screening length

$$\kappa^{-1} = \sqrt{\frac{\epsilon k_{\mathrm{B}} T}{8\pi n \nu^2 e^2}}\ , \tag{11}$$

where ϵ is the dielectric constant of the medium, n the concentrations of ions, ν the ion valency, e the elementary charge, k_{B} the Boltzmann constant and T the temperature [135]. As in experiments, the drop is held at the top and deforms under gravity, but the particle weight is ignored and the particle to initial-drop radius is relatively small at 0.02 (though sufficient to achieve separation of length scales). The surface tension is then calculated in two ways:

(i) calculating the local surface stress by local spatial averaging using an extension of the Irving-Kirkwood expression [136];

(ii) fitting the shape of the composite interface to a solution of the non-linear Young-Laplace equation (this is similar to the procedure used in most experiments to measure an effective surface tension).

The authors find that, for parameters that do not result in droplet pinch-off, the two methods agree i.e. the surface stress is homogeneous and isotropic (so for coverages $<$ 0.5 and the charged particles studied here the surface can be characterized by a single value for its tension). This is in line with the observations that for such charged particles extra and deviatoric contributions to the surface stresses only really 'kick in' close to maximum packing [137].

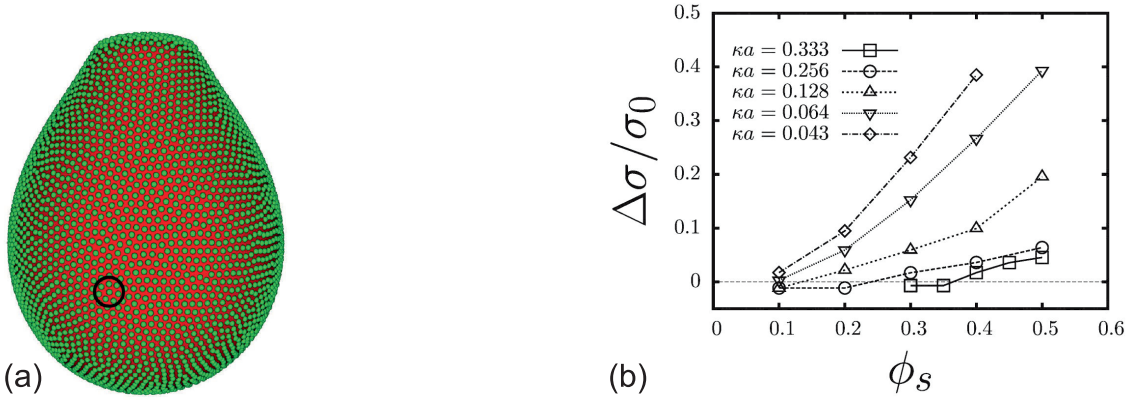

Figure 8. (a) Simulation snapshot of steady-state drop shape for a surface coverage of 45% charge-stabilized particles with a screening length of $\kappa^{-1} \approx 15.6a$ (particle radius a); the circle indicates a disclination in the crystal structure. (b) Surface pressure $\Delta\sigma$ versus area fraction for a pendant droplet covered with particles for different values of the screening length κ. Both panels adapted from Ref. [134].

The simulations also show that surface pressure is affected by particle polydispersity and clustering. Moreover, it has a strong dependence on surface coverage ϕ_s, i.e. increasing coverage or interaction strength/range gives a larger surface pressure. In fact, they provide a way to estimate the lowest coverage $\phi_{s,min}$ required to get a finite surface pressure. For hexagonally packed particles, the average distance between particles

$$l = \sqrt{\frac{2\pi a^2}{\sqrt{3}\phi_s}} \ . \tag{12}$$

An estimate for $\phi_{s,min}$ can be acquired by setting $l = \kappa^{-1}$, resulting in

$$\phi_{s,min} = \frac{2\pi}{\sqrt{3}} (\kappa a)^2 \ . \tag{13}$$

Using the values provided by Ref. [133], we estimate that $\kappa^{-1} \approx 0.27$ nm in their case, i.e. $\kappa a >> 1$. Looking at figure 8(b), this means a surface coverage close to unity would be required for $\Pi > 0$ and, as there is no guarantee that a close-packed layer assembles on the water-oil interface without contracting the droplet, this may explain why no change in apparent interfacial tension was measured in Ref. [133].

Gu and Botto also note that particle expulsion or ejection can occur, but only under conditions of large surface coverage and/or relatively weak particle adsorption. Experimentally, this corresponds to particles with a small radius (nanoparticles) and/or with a contact angle θ close to 0 or 180°. Their transient simulations suggest that, in the case of unstable droplets, i.e. droplets that eventually pinch off, anisotropic stresses mainly concentrate in the neck region of the pendant droplet; this aligns with experimental observations of wrinkle formation in the neck region of a pendant drop upon sufficient

contraction [41, 138].

Finally, the authors make a valid point about results for curved surfaces being more difficult to interpret than for flat surfaces. However, they also point out that these results are more realistic, as they account for the two-way coupling of the distribution of particles across the liquid interface and the shape (or curvature) of the interface. Indeed, Tavacoli *et al.* [132] have shown that Pickering droplets in gravity have a maximum size because their curvature leads to out-of-plane components of the interparticle forces and these can accumulate at 'keystone' particles. In their words, "a single keystone particle gets ejected under the cumulative body force of a patch of particles bearing down upon it" [132]. Notably, they observed that particle ejection was mainly localized in regions of high curvature, supporting the notion that curvature, and the associated out-of-surface interparticle forces, are pivotal. These results align with the work by Garbin *et al.* [128], who showed that gold nanoparticles are forced off the interface at the underside of a pendant drop upon compression, though the authors caution that the ligands capping the gold nanoparticles are likely to play a crucial role in their experiments.

In short, a limited number of papers have reported pendant-drop measurements for IDC PS-S particles. From the few we have found, we deduce that the particles do not change the apparent interfacial tension at surface coverages well below close packing. Upon close packing, the pressure-area isotherms deviate from those recorded using a Langmuir trough and it has been suggested that the curvature of the drop could lead to particle ejection. As suggested by Aveyard *et al.* [127], we would emphasize here that the Laplace equation, used in the analysis of the drop profile to extract tension, may not apply to the potentially rigid interfaces formed upon compression. A more elaborate analysis either based on drop shape elastometry [41] or stress fitting tensiometry [39] would be required to properly deconvolute the mechanical effects from those related to the thermodynamic state variables.

All in all, the isotherms or apparent isotherms of surface pressure versus area measured using throughs or with the pendant-drop instrument reveal that particle monolayers can likely generate very high values of Ma and Bo_{d}. For repulsive, near-hard sphere systems, the incompressibility will be the main factor responsible for generating large values of $\mathrm{d}\Pi/\mathrm{d}A$ near maximum packing. For aggregated systems, the network structures will give rise to significant surface stress in compression from the onset of percolation onwards, but the slopes of the pressure-area isotherms will typically be less steep. The slopes are then controlled by both changes in the thermodynamic parts, as well as extra mechanical stresses due to the compressional strength of the particle networks. Hence, there are different methods to engineer this response and impart PE/bijel stability, which will further discuss in section 4.

3.3. Shear rheology

So far, we have focussed on dilational rheology, but it is important to consider shear rheology as well. The rheological properties in shear will reflect the resistance of the interface to changes in shape rather than area, and this will also play a role in bijel structuring (through the Boussinesq number Bo_s). Secondly, when shear rheology is measured as a function of surface coverage, the point where a finite shear modulus is measured can be identified as the point where solid behaviour starts to emerge; this is also the point where extra stresses can be expected under compression. As shear rheology only picks up the deviatoric part of the stress it can be used more as an analytical technique, in the spirit of mechanical spectroscopy, to elucidate structure-property relations.

As an example of elucidating structure-property relations in particle monolayers, Stancik *et al.* [139] used a dual-band surface shear cell, with an optical microscope attached, to deform an interfacial hexagonal crystal of PS-S particles with spacing significantly larger than the particle diameter due to the electrostatic dipole-dipole repulsion. They used monodisperse spherical IDC PS-S particles, with diameter 3.0 μm and surface charge density 7.5 $\mu\mathrm{C}\cdot\mathrm{cm}^{-2}$, at an interface between decane and water with 10 mM NaCl. At low surface coverage or high shear rate, they observed strings of particles aligning in the flow direction, the overall structure as determined by Fourier Transforms (FTs) being that of a stretched hexagonal crystal. At high coverage or low shear rate, the particles remain in their lattice positions, leading to the rotation of domains; they observed cyclic melting and crystallization under flow. They explain their observations by a balance between flow and interparticle forces i.e. particles are closer together at high surface coverage and therefore interact more strongly. It is a prime example of how the interfacial structure responds to deformation and motivated further research into the rheology of colloid monolayers.

Reynaert *et al.* [137] confirmed the importance of interparticle interactions on interfacial rheology. They used a magnetic needle surface rheometer to study IDC PS-S particles, with a diameter of (3.1 ± 0.2) μm and a surface-charge density of 7.8 $\mu\mathrm{C}\cdot\mathrm{cm}^{-2}$, both at water-air and water-decane interfaces; we focus here on the latter given its potential relevance to bijels. They start with a stable interfacial crystal and then destabilize it using 0.1 M NaCl and 0.1 mM sodium dodecyl sulfate (SDS) to weaken the dipole-dipole interactions. Note that a major benefit of their system is that the interparticle potential has been measured by optical tweezers and the effects of the surfactant SDS on interfacial tension and contact angle are known [109, 123]. Upon increasing surface coverage, the aggregated structure goes from a fractal network to a heterogeneous structure with voids, a gel with dense clusters and eventually a densely packed system with small crystalline patches. The authors show that surface coverage and interparticle interactions can be used to tune the visco-elastic properties of the interface under shear

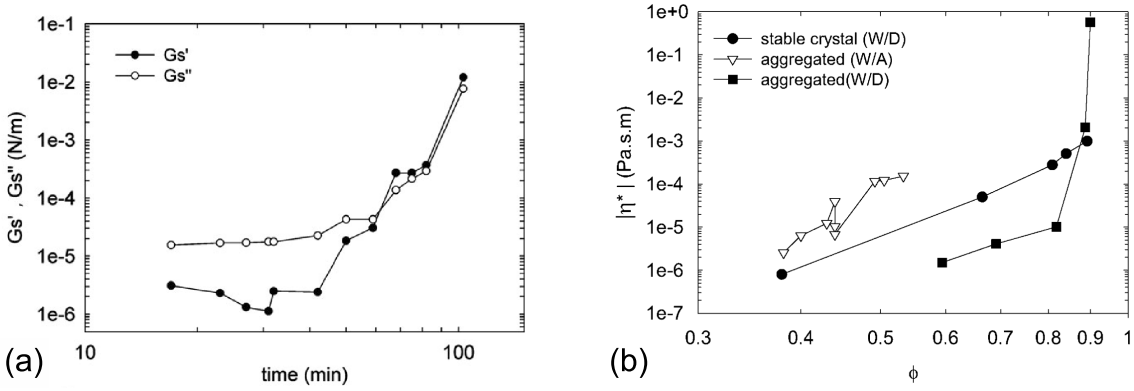

Figure 9. (a) Change in surface elastic $G_s^{'}$ and viscous $G_s^{''}$ moduli at 0.1 Hz over time for a dense monolayer of 3.1 μm diameter IDC PS-S particles at a water-air interface; the initial colloidal crystal was destabilized by adding 0.1 mM SDS and 0.1 M NaCl to the water phase. (b) Magnitude of complex viscosity versus surface coverage ϕ for the same particles at a water-decane interface, with 0.1 mM SDS and 0.1 M NaCl added to the water phase ("aggregated (W/D)"). Both panels adapted from Ref. [137].

over a larger range (figure 9). Notably, the aggregated structures can have solid-like rheological properties at low surface coverage, but they are brittle i.e. have low yield strains (yielding in this system was studied in more detail by Masschaele *et al* [140]).

One disadvantage of the magnetic needle surface rheometer is that, given a specific needle, it has a relatively small dynamic range [46]. The double-wall ring has similar sensitivity and relatively large dynamic range, but is conventionally not coupled to a microscope [46]. Barman *et al.* [44] combined a double-wall ring (DWR), attached to a Langmuir trough to control surface coverage, and brightfield microscopy to investigate interfacial microstructure under steady shear. They used IDC-PS particles of diameter (3.1 ± 0.2) μm and surface-charge density 7.8 $\mu\mathrm{C} \cdot \mathrm{cm}^{-2}$ at an aqueous phase-air interface (contact angle 117°). The subphase was a mixture of water and glycerine (30%) to match the density of polystyrene and thereby prevent particle sedimentation; NaCl was included at 0.4 M. Using FTs of micrographs (figure 10(a)), they find a hexatic phase at high coverage, i.e. local sixfold symmetry but no long-range hexagonal ordering, which turns crystalline at high shear rates. They also observe a transition from shear thinning to yielding upon increasing coverage but before jamming occurs at 77% (figure 10(b)), which suggests the system is attraction dominated; microscopy reveals that yielding corresponds to the interface moving as a single unit i.e. not following the DWR flow profile. Perhaps confusingly, the authors describe the yielding microscopically as the emergence of a slip plane between a high and a low-shear zone, which one could interpret as shear banding [141] rather than yielding. As before, interparticle interactions play an important role: the observations can be explained by balancing a long-range capillary attractive force caused by contact-line undulation [108, 123, 142, 143] and a re-

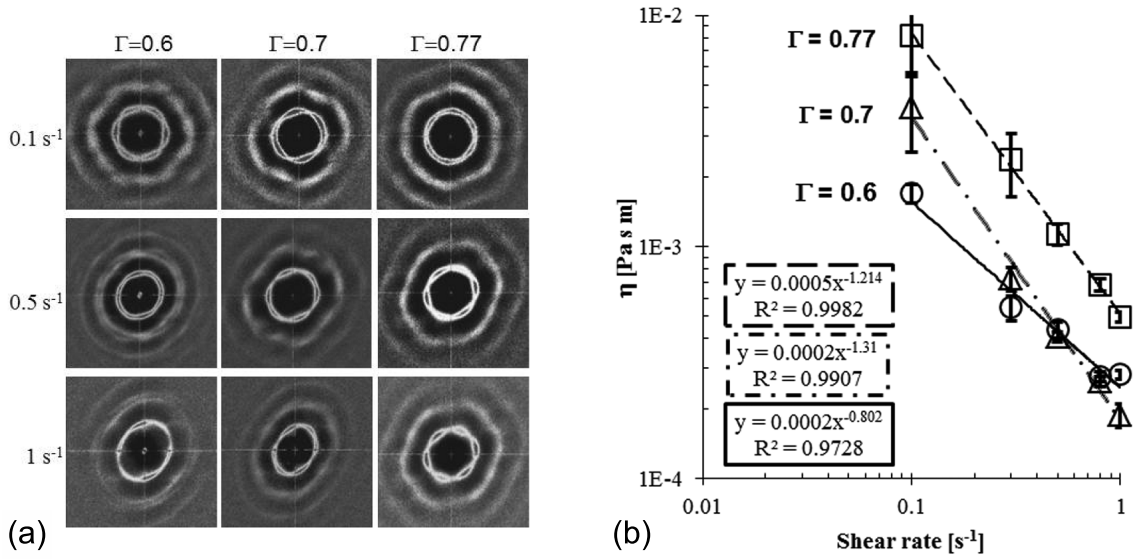

Figure 10. (a) Typical Fast Fourier Transforms of micrographs, corresponding to shear rates of 0.1, 0.5 and 1 s^{-1}, for 3.1 μm diameter IDC PS-S particles at surface coverage Γ at a an interface between air and water-glycerine with 0.4 M NaCl. (b) Interfacial viscosity versus shear rate for a similar interface. Both panels adapted from Ref. [44].

pulsive dipole interaction [108, 123]. Resistance to flow can then come from aggregation forming a percolating network or from caging due to crowding effects at high surface coverage.

In a follow-up paper, Barman *et al.* [144] further investigate the correlation between interparticle forces, microstructure and rheology by changing salt concentration and surface-coverage for the same system under oscillatory shear (figure 11(a)). They find that adding more salt leads to stronger interparticle attraction, which they attribute to screening of the dipole repulsive interaction. At high salt, increasing coverage also leads to higher moduli, suggesting that crowding, and possibly caging, plays an additional role. These two observations suggest that the magnitude of the moduli is determined locally by the degree of restriction of particle motion, either by attractive capillary forces or by the severity of caging (figure 11(b)). However, qualitative rheological trends like elasticity and yielding are determined by mesoscale organization i.e. large domains of hexagonally packed particles create elastic interfaces, which turn viscous when large domains break up into smaller domains. Intriguingly, the authors find (even at high coverage) a transition from hexagonal to hexatic ordering with increasing strain; similar to flow in solids being due to defect motion [145].

Even though inspired by jamming rather than PR-emulsion stability, a paper by Keim *et al.* [146] introduces an different way to define yielding that is worth mentioning

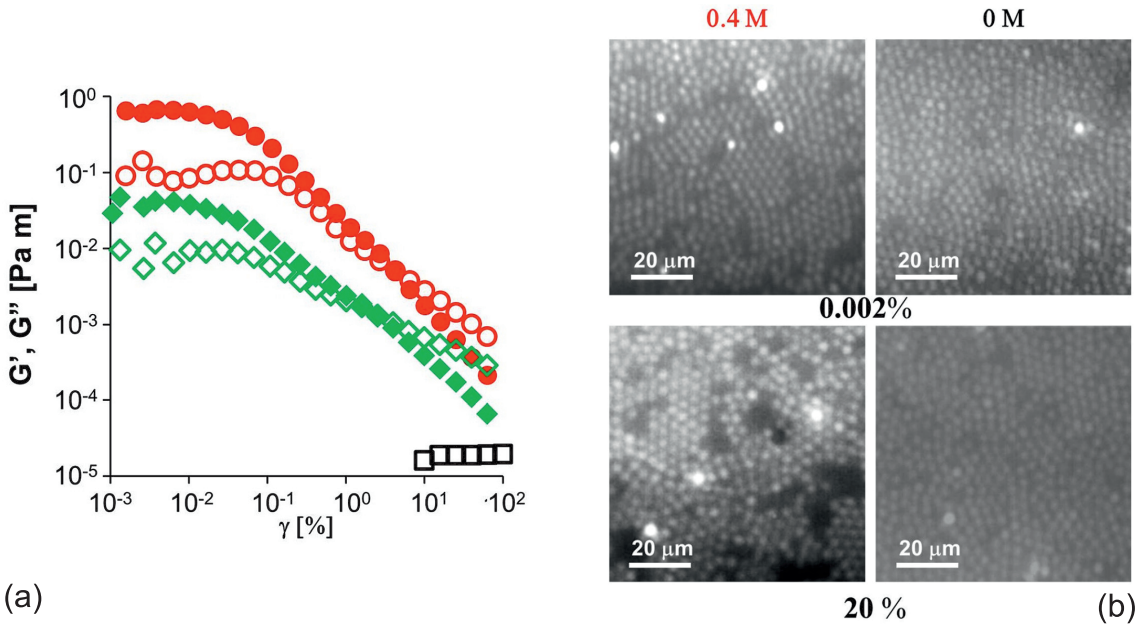

Figure 11. (a) Storage (solid) and loss (open) moduli at 1 rad/s for 3.1 μm diameter IDC PS-S particles at surface coverage 79% at a an interface between air and water-glycerine with 0.4 M NaCl (circles), 0.004 M NaCl (diamonds) and 0 M NaCl (squares). (b) Interfacial micrographs for 0.4 M and 0 M NaCl at a surface coverage of 79% at 0.002% and 20% strain. Both panels adapted from Ref. [144].

here. They used PS-S particles from Invitrogen, a bi-disperse system of 4.1 and 5.6 μm diameter, non-Brownian particles at a water-decane interface at a surface coverage of 43% i.e. just above the jamming transition. Using a magnetic-rod interfacial-stress rheometer, they perform cyclic rheometry at 0.1 and 0.2 Hz, using particle tracking to obtain stress-strain curves and count T1 events (where particles switch neighbours). They conclude that: "the bulk yielding transition corresponds to the largest cyclic deformation that leaves microstructure unchanged" [146]. This microscopic view on dynamic yielding may be an alternative to criteria used in conventional interfacial rheometry e.g. IFR or DWR [53]. Squires and coworkers used a microdisk forced to rotate at a controlled angular velocity; the nonlinear shear-rate-dependent surface viscosity of the PS-S monolayers can be extracted from a local interfacial stress balance [147]. This technique was further used by Buttoni and coworkers and revealed how particles showing high deviatoric stresses are localized around grain boundaries and defects, providing a simple criterion to spot regions likely to rearrange plastically under oscillatory shear [148]. It would be extremely interesting to see how monolayers with different structures (e.g. aggregated versus liquid-like) react to deformations, but studies combining visualization and non-linear rheology are clearly bringing detailed insights into the deformation and flow mechanisms.

In conclusion, shear rheology has been extremely useful in detecting the emergence of solid-like properties in colloidal monolayers. Most focus so far has been on the linear properties or the steady-state properties, even though understanding how the yielding behaviour can be controlled is probably important for these systems as well. Interestingly, many interfacial shear-rheology papers claim relevance to the stability of PR emulsions, even though the exact nature of this relationship is still not completely clear [55]; we will return to this discussion in section 4.

3.4. Bending stiffness

Besides the mechanical properties of particle-laden interfaces under compression and shear, bending should be considered as well. Properties related to bending of particle monolayers are usually obtained from a wrinkling analysis [40, 41]. Typically, bending moduli are relative small compared to dilatational and shear moduli [53, 149]. However, that does not mean bending plays no role in the formation and/or stability of (bicontinuous) Pickering emulsions (section 4). For example, Reeves *et al.* explain why bijel formation is more robust using nanoparticles rather than microparticles by considering the bending of the particle-laden interface [72]. In addition, theoretical work by Kralchevsky *et al.* has shown that bending energies of close-packed particle monolayers could cause flocculation of particle-coated droplets [150].

Vella *et al.* [40] studied a variety of non-Brownian particles at a water-air interface, including polystyrene powders of different grain sizes 300 μm $< d <$ 7 mm. Under uniaxial compression in a Langmuir trough, they observed wrinkling (see also section 3.1), which disappeared after removing the compressive stress. Theoretically, they describe the particle raft as an isotropic, 2D, elastic solid with a Young's modulus E and a Poisson ratio ν. Assuming rigid spherical particles, they modify an argument by Lucassen [151] to derive an expression for the Young's modulus

$$E \propto \left(\frac{1-\nu}{1-\phi}\right)\left(\frac{\gamma}{d}\right) \ , \tag{14}$$

where ϕ is the particle surface fraction and γ the surface tension. To describe the wrinkling, they continue by using the beam equation [152] to derive an equation for the wrinkling wavelength

$$\lambda = \pi\left(\frac{16B}{\rho g}\right)^{1/4} \ , \tag{15}$$

in which $B = Ed^3/12\,(1-\nu^2)$ is the bending stiffness of the particle raft, ρ the density of the liquid and g the acceleration due to gravity. Assuming the particles go from a hexagonal to a rhombic packing under compression, their experimental wrinkling wavelengths compare favourably to this theoretical model.

Kassuga *et al.* [149] extended this work to particles at water-oil(decane) interfaces in a Langmuir trough combined with light-sheet microscopy; it should be noted that they used a micrometer to control interfacial compression i.e. the strain was precisely controlled but not the strain rate. They mainly used polystyrene particles, including PS-S, with sizes spanning 0.1 to 10 μm. They also observe wrinkling and provide a clear physical picture: a particle-laden interface buckles if local bending is energetically more favorable than further compressive deformation with additional in-plane strain; given that the particles are typically rigid and the bending stiffness of a particle raft tends to be relatively small, a particle raft will usually buckle given enough strain. The measurements by Kassuga *et al.* confirm Vella's model for particles larger than 0.8 μm, but they find wavelengths larger than expected for sub-micron particles. They suggest the deviation is due to the formation of trilayers: these would have a higher effective bending stiffness than monolayers and this would lead to larger wrinkling wavelengths. Furthermore, they show that the strain history can affect the critical strain at which wrinkles appear, as well as their uniformity and wavelength, which they attribute to changes in particle packing between successive cycles. For GO particles, which were used by Imperiali *et al.* in the formation of bijels [58], very low bending moduli were inferred from a buckling analysis. The resistance of those GO layers was similar to the bending elasticity of surfactant films.

Using silica rather than polystyrene particles at water-air interfaces, Planchette *et al.* [153] investigate capillary wave propagation as an alternative method to measure the mechanical properties of particle rafts; they avoid the macroscopic wrinkling discussed above by working at a surface fraction just above that required for close packing. They excite the particle raft using a vertically oscillating glass plate and extract the stretching modulus and the bending stiffness of the particle raft, at frequencies between 100 and 900 Hz, from measurements of wave phase speed versus wave vector. For particles with diameters between 35 and 159 μm, they find that the stretching modulus does not vary with particle size r, whereas the bending stiffness varies as r^2; note that this size dependence agrees with Vella's theory [40]. The contact-angle dependence is captured by a theoretical argument modified from Kralchevsky *et al.* [150] and Aveyard *et al.* [154], though the experimental bending stiffness is systematically smaller than the predictions, which they attribute to (projected) particle overlap or contact-angle hysteresis.

In conclusion, the occurrence of monolayer buckling suggests that the monolayers can be approximated as near 2D solids at sufficiently high surface coverages, and the analsysis shows that bending moduli for such particle layers are relative small compared to dilatational and shear moduli.

4. Role of interfacial rheology in simple and bicontinuous Pickering systems

4.1. Pickering emulsions

We start our discussion of how interfacial rheology affects PE stability by first considering emulsions formed via limited coalescence [155–157], as this tallies with bijel formation in the sense that initially there are insufficient particles to fully cover the oil-water interface [62]. Initially, at low surface coverage ($\phi \ll 40\%$), the effective surface viscosity η_s of particle-laden interfaces is low ($\eta_s \ll 10^{-6}$ Pa $\cdot$ s $\cdot$ m) (figure 9) [137], whereas the bulk viscosity $\eta \sim 10^{-3}$ Pa $\cdot$ s (water) is a fixed value [24]. In equation (3), $Bo_s = \eta_s/(\eta a)$, the value a is the characteristic length scale over which the velocity decays at the interface [35]. As 1 μm $\lesssim a \lesssim$ 10 μm is between the particle and the droplet radius, the Boussinesq number $Bo_s << 100$, which means the mechanical properties of the interface do not dominate and cannot prevent further coarsening via coalescence.

As particles are irreversibly attached (equation (1)), surface coverage increases as coarsening proceeds, which also means that surface viscoelastic moduli increase in magnitude. At some point, the Boussinesq number(s) $Bo_s >> 1$ and the mechanical properties of the interface start dominating bulk flows. If the particles aggregate in bulk and/or at the interface, this point can be reached well before close packing of particles at the droplet interface i.e. when $\Pi < \gamma$ [13]. We first consider the case where interfacial-shear rheology dominates, i.e. $\Theta = \kappa_s/\eta_s << 1$. Expressing the Marangoni number (equation (7)) in terms of Θ,

$$Ma = \frac{K\Gamma_0}{\eta^s \dot{\gamma}_{\,s}} = \frac{K\Gamma_0\Theta}{\kappa_s \dot{\gamma}_s} \,, \tag{16}$$

in which K is the slope of the isotherm and Γ_0 the equilibrium surface coverage at a surface pressure Π, while κ_s is the surface dilatational viscosity and $\dot{\gamma}_s$ the shear rate [35]. For $\Theta << 1$, the Marrangoni number may still be small when K is not too big, and $Ma << 1$. This implies that redistribution of particles will be difficult. Whereas there can still be a driving force towards further coarsening ($\Pi < \gamma$), droplet coalescence requires particle redistribution and the particle-laden interface renders the required flow difficult. Note that, in this interfacial-shear dominated scenario, PE stabilization may be enhanced by particles that aggregate in the bulk and/or at the interface, as suggested by various studies [11, 56, 57].

Alternatively, surface-dilatational properties may lead to $\Theta >> 1$ and hence typically $Ma >> 1$. In this case, redistribution of interfacial particles is hardly opposed and so coarsening via coalescence will proceed. This will continue until the surface coverage approaches close packing, or effective close packing in the case of particles with long-range repulsive interactions. At that point, the effective surface pressure Π is equal to the bare liquid-liquid interfacial tension γ (figure 3), which means the apparent interfacial tension is 0 and the driving force for further coarsening vanishes (including

coarsening via Ostwald ripening [8]). Droplet coalescence would result in a higher surface coverage on the merged droplet and the relatively high (effective) surface pressure makes this energetically unfavourable. Note that in this scenario, particles need not aggregate in bulk and/or at the interface to achieve PE stability, as argued by Van Hooghten *et al.* [55].

In non-quiescent conditions, the particle-laden surfaces of two colliding droplets may have dilated, resulting in a lower surface pressure i.e. the two deformed droplets could merge. Upon cessation of the external flow field, the merged droplet will relax towards a spherical shape, but it can get stuck in a non-spherical shape if the effective surface pressure of the particles on the merged droplet reaches γ *en route*; non-spherical droplets/bubbles have indeed been observed after coalescence of Pickering droplets/bubbles [158–161].

There are various other mechanisms that contribute to PE stability by impeding droplets from colliding in the first place. First, if the droplets and/or the particles are charged, the PE droplets can repel via electrostatic interactions, especially if those are unscreened e.g. in the case of a continuous oil phase. Secondly, Tambe and Sharma [162] have shown that the viscoelastic properties of particle-laden droplet surfaces can inhibit drainage i.e. the process of liquid moving out of the interdroplet film. Moreover, particles that aggregate in the continuous phase can endow it with viscoelastic properties, effectively trapping the droplets in a matrix [11]. Finally, droplets can share particles via bridging, which in some cases can enhance PE stability [163].

4.2. Bijels i.e. bicontinuous Pickering emulsions

The main structural difference between PEs and bijels, or bicontinuous Pickering emulsions, is that the former consist of discrete droplets in a continuous phase, whereas the latter consist of two continuous, interpenetrating channels (figure 1). Conventionally, bijels are formed by spinodal decomposition of a binary liquid in the presence of colloidal particles. As in the case of PEs formed by limited coalescence, there are initially insufficient particles to fully cover the (spinodal) liquid-liquid interface. As argued in section 4.1, this results in relatively low Boussinesq numbers i.e. the mechanical properties of the interface initially do not dominate and cannot prevent further coarsening. As phase separation proceeds, the interfacial coverage of particles increases for two reasons:

(i) adsorption of particles from the bulk liquid phase(s);

(ii) the decrease in available liquid-liquid contact area (particularly relevant in the later stages).

At some point, the structure percolates laterally and the interfacial-particle layer starts to build up stress and impede further coarsening. Given the convoluted nature of the

spinodal interface, we expect a complex interplay between dilatational rheology, curvature, shear rheology and bending; we attempt to unpick this below.

Imperiali *et al.* [58] were the first to discuss the role of interfacial rheology in bijel formation, in particular water-lutidine bijels stabilized by graphene-oxide (GO) platelets. They argued that, at some point during phase separation, the GO sheets percolate laterally and the interfacial-particle layer compresses until it builds up sufficient *compressional* stress to resist further coarsening. From an experimental point of view, compressional interfacial rheology for particle layers can be characterized, for example, with Langmuir-trough pressure-area isotherms. From section 3.1, we highlight two results that appear particularly relevant here. First, colloidal particles are unlikely to be ejected from a (flat) liquid interface upon monolayer compression. If this were not the case, it would result in particle ejection in bijels, and hence to further coarsening, which has not been observed. Secondly, compression of particle monolayers at flat liquid interfaces can lead to surface stresses as large as the liquid-liquid interfacial tension, which means the apparent interfacial tension vanishes.

Due to relatively strong evaporation of the lutidine, Imperiali *et al.* [58] could not measure the interfacial rheology of GO particles at the interface between water-rich and lutidine-rich phases. Instead, Langmuir-trough measurements on similar GO particles at a water-air interface [53] were used to rationalize the observations. From that data, Imperiali *et al.* extract the compressive modulus

$$K_{\mathrm{int}} = -A\frac{\mathrm{d}\Pi}{\mathrm{d}A} = -\frac{\mathrm{d}\Pi}{\mathrm{d}\left(\ln A\right)} \approx -\frac{\Pi_1 - \Pi_2}{\ln A_1 - \ln A_2} \ , \tag{17}$$

where A is the liquid-interfacial area available to the particles and

$$\Pi = \gamma_0 - \gamma_{\mathrm{p}} \tag{18}$$

is the surface pressure, with γ_0 the interfacial tension of the bare water-oil interface and γ_{p} the (apparent) interfacial tension of the particle-laden interface. It was shown that K_{int} rises steeply at the area at which the particles percolate laterally A_{PT} and reaches a maximum at $A \approx 0.9 \cdot A_{\mathrm{PT}}$. The value of K_{int} at its maximum is $\sim 10^2\ \mathrm{mN \cdot m^{-1}} \gtrsim 72\ \mathrm{mN \cdot m^{-1}} = \gamma_{\mathrm{water-air}}$ [24]. As γ drives the coarsening and K opposes the deformations associated with coarsening, the authors argue that the interface becomes mechanically so robust that it can hinder further phase separation.

However, some of these arguments may be specific to the GO particles used. When the interaction potential is attractive, the percolation threshold will indeed agree with the point at which particles start to impart surface stresses. But for example for hard-sphere suspensions, the surface pressure (or more precise the overall surface stress) will only start to rise when the particles near close packing, which will be at surface coverages well beyond A_{PT}. Also, the discussion so far ignores any effect of curvature, which can be probed experimentally by pendant-drop measurements. In section 3.2, we

saw that (effective) pressure-area isotherms recorded by pendant drop and Langmuir trough can differ and it has been suggested that the curvature of the drop could lead to particle ejection. Should this observation transfer to bijel formation, it would mean that particles could be ejected from the bijel surface during formation, i.e. they would not be able to halt liquid-liquid demixing, which does not align with observations from bijel simulations and experiments.

A potential way out of this conundrum is the "keystone mechanism" for Pickering droplets suggested by Tavacoli *et al.* [132], i.e. curvature leads to out-of-plane components of the interparticle forces and these forces can accumulate at keystone particles, leading to their expulsion from the interface. This keystone mechanism may also be relevant to the formation of bijels, as they only have an area-averaged mean curvature $\langle H \rangle$ close or equal to 0 [118], i.e. they are not minimal surfaces with $H = 0$ for each point on the interface. This could be an important distinction: particles could be expelled from those regions of the bijel surface that have high (local) curvature. However, given that the bijel surface has points of positive and points of negative mean curvature, it is unclear whether a keystone particle could be defined and, hence, whether similar collective effects play a role in bijel stability. Anisotropic stresses (for non-spherical particles) [164] and further coarsening (for small nanoparticles) [62] have been observed in bijel simulations and curvature changes have been observed in experiments up to an hour after bijel formation [118]. However, there is currently no experimental evidence of further coarsening, which seems to suggest that particles are not being expelled from the bijel surface (at least not for the particle-size range 50 nm $< r <$ 367 nm explored) [63, 72, 118].

Having discussed dilatational rheology, we considered shear rheology in section 3.3 and concluded that it is in addition particularly useful as an analytical tool. As only the deviatoric stresses are measured, shear properties as a function of surface coverage will be useful in identifying when solid-like behaviour is imparted to the interface, by appearance of a surface shear modulus. Unfortunately, the relevance of shear rheology to bijel formation is difficult to ascertain. Initially, the particles at the interface will be far apart and so the role of interfacial shear rheology will be negligible. Upon coarsening, the surface coverage of particles increases, meaning that percolation by aggregation or caging might occur; this could slow down or even halt phase separation. Viscous effects can only slow down phase separation, whereas simulations have shown that particle-induced elastic forces can halt phase separation [165, 166]. Notably, aggregated structures can have solid-like shear rheological properties at low surface coverage, but they are brittle i.e. have low yield strains. Though an interface with solid-like properties is required for bijel formation, it is unclear whether a brittle surface could bend both ways to accommodate the spinodal structure.

Finally, in section 3.4, we reviewed literature on the bending modulus of particle-laden liquid interfaces. Though interesting from an interfacial-rheology point of view, it is not clear what role bending plays in bijel formation. During the later stages of bijel formation, but before the interfacial particles are closely packed, the surface coverage increases due to a reduction of liquid-liquid contact area. At any given surface coverage, the system has two options: i) contract without bending or ii) bend without contracting. The latter is energetically unfavorable, as it incurs an energy penalty without a reduction in interfacial energy from reduction of liquid-liquid contact area. The former, on the other hand, is energetically favorable as long as the effective surface pressure Π is smaller than the liquid-liquid interfacial tension γ. As soon as $\Pi \sim \gamma$, the driving force for further contraction disappears and the bijel stops coarsening. Note that this is different from a Langmuir-trough experiment, in which a compressive force is provided by the barriers even if $\Pi \sim \gamma$. This difference may well explain why buckling is observed in Langmuir-trough and pendant-drop experiments, but not in bijel formation. However, this does not mean that bending considerations do not play a role in bijel formation at all, as they can explain i) bijels forming more easily using smaller particles [72] and ii) curvature changes after bijel formation [118].

Clearly, further research is needed to translate observations from particles at planar fluid-fluid interfaces, or those with positive Gaussian curvature (e.g. droplets), to bijel systems. This applies to experiments and simulations, but also to theoretical models. For example, Reeves *et al.* [72] have reported some initial theoretical considerations to explain why nanoparticles are better at locking in the spinodal-decomposition pattern than microparticles. They suggest that, even though microparticles demand a more modest curvature, the driving force towards that curvature is larger. Hence, off-neutral microparticles can induce curvature to such an extent, before interfacial jamming, that it prevents bijel formation. However, more theoretical research is required to refine or improve upon these ideas. In addition, various simulation efforts have been instrumental in qualitatively explaining observations and suggesting interesting avenues for experimental research, but a quantitative mapping is still lacking, partly because the maximum particle size that can be simulated is an order of magnitude smaller than the minimum particle size (typically) achievable in experiments. Having said that, simulation methods to obtain realistic results for more complex interfacial systems have recently been reviewed [167].

5. Summary and outlook

In this review, we have summarized the literature on the interfacial rheology of model-particle monolayers at liquid-liquid interfaces. Interfacial-rheology results from literature are difficult to compare due to the variety of particles used, which affects interparticle and particle-liquid interactions. Hence, we have focussed on (IDC) polystyrene-sulfate particles, as these have been extensively used and are well-characterized. More-

over, we have considered the relevance of the findings reported to the formation and stability of Pickering emulsions and bijels (bicontinuous Pickering emulsions).

Reviewing Langmuir-trough results, we have established that colloidal particles are unlikely to be ejected from flat liquid interfaces upon compression and this aligns with observations that bijels do not coarsen after their formation. Comparing Langmuir-trough to pendant-drop data, it has been suggested that particle ejection might be possible in the case of curved liquid interfaces. However, this comparison is not straightforward. First, the Laplace equation typically used in drop-profile analyses may not always apply to particle-laden liquid interfaces [127]. This has recently been explored using computer simulations [134] and methods recently became available to deal with this challenge [39]. Secondly, the measured surface pressure contains contributions related to the changes in the equilibrium properties as well as the compressional elasticity of a structured interface (we have used 'effective surface pressure' to describe this quantity). In this respect, stable suspensions will react differently than aggregated ones. All the same, it has been confirmed by optical methods that particles can be forced off the underside of a pendant drop [128].

Bijel formation mainly relies on *compression* of the interfacial-particle layer until it resists further coarsening and, hence, the thermodynamic compressibility and dilatational rheology are expected to be pivotal (Ma and Bo). However, interfacial shear rheology may also play an important role, e.g. through its coupling to bulk flows in the bijel channels, as it also appears in the stress boundary condition. In addition, when the shear properties are negligible, it will be easy for the interface to start deforming and changing shape, which can be expected to facilitate breakup of the spinodal pattern into droplets. Clearly more intricate engineering of the non-linear rheological properties could lead to better designed bijels. However, little is known about these non-linear rheological properties as yet.

Given that it may not be trivial to translate observations from interfacial-rheology set-ups to bijel systems, an interesting path is to develop in-situ interfacial-rheology methods for bijel surfaces. Most interfacial macro-rheology methods require probes of order 1 mm and these are simply too large given the channel widths and curvatures in bijels. Moreover, interfacial rheology measurements are dominated by bulk flows unless the Boussinesq number Bo (equation (3)) is of order 10 or larger. As $Bo = \frac{\eta_s}{\eta a}$, with a a dimension related to the measurement set-up, it may well be necessary in bijel systems to move to $a << 1$ mm if the surface viscosity is significantly smaller than 10^{-5} Pa·m.

In short, we expect that measuring interfacial rheology in bijel systems will be challenging and will require micro-rheological techniques. Even though initial attempts have been reported, this also means more effort is required to align interfacial micro-rheological and macro-rheological methods, as the two often disagree by orders of

magnitude and rationalizing the difference is not trivial [168]. Hence, we expect that techniques including diffuse-wave spectroscopy, differential dynamic microscopy and fast confocal microscopy, or techniques which couple the observations of the particulate microstructure to the response of the macroscopic bijel structure, are an interesting path forward.

Acknowledgements

J. H. J. T. acknowledges A. Brown for useful discussions and The University of Edinburgh for a Chancellor's Fellowship.

6. References

[1] P. Colombo, C. Vakifahmetoglu, and S. Costacurta. Fabrication of ceramic components with hierarchical porosity. *Journal of Materials Science*, 45:5425–5455, 2010.

[2] B. P. Binks, editor. *Modern Aspects of Emulsion Science*. The Royal Society of Chemistry, Cambridge (UK), 1998.

[3] F. Leal-Calderon, J. Bibette, and V. Schmitt. *Emulsion Science - Basic Principles*. Springer Verlag, New York, 2007.

[4] T. N. Hunter, R. J. Pugh, G. V. Franks, and G. J. Jameson. The role of particles in stabilising foams and emulsions. *Advances in Colloid and Interface Science*, 137:57–81, 2008.

[5] F. Leal-Calderon and V. Schmitt. Solid-stabilized emulsions. *Current Opinion in Colloid & Interface Science*, 13:217–227, 2008.

[6] R. A. L. Jones. *Soft Condensed Matter*. Oxford University Press, Oxford (UK), 2002.

[7] P. J. Wilde. Interfaces: their role in foam and emulsion behaviour. *Current Opinion in Colloid & Interface Science*, 5:176–181, 2000.

[8] S. Tcholakova, N. D. Denkov, and A. Lips. Comparison of solid particles, globular proteins and surfactants as emulsifiers. *Physical Chemistry Chemical Physics*, 10:1608–1627, 2008.

[9] W. Ramsden. "separation of solids in the surface-layers of solutions and 'suspensions' (observations on surface-membranes, bubbles, emulsions, and mechanical coagulation). preliminary account.". *Proceedings of the Royal Society of London*, 72:156–164, 1903.

[10] S. U. Pickering. Emulsions. *Journal of the Chemical Society*, 91:2001–2021, 1907.

[11] B. P. Binks. Particles as surfactants - similarities and differences. *Current Opinion in Colloid & Interface Science*, 7:21–41, 2002.

[12] Y. Chevalier and M. A. Bolzinger. Emulsions stabilized with solid nanoparticles: Pickering emulsions. *Colloids and Surfaces A-Physicochemical and Engineering Aspects*, 439:23–34, 2013.

[13] B. P. Binks and T. S. Horozov, editors. *Colloidal Particles at Liquid Interfaces*. Cambridge University Press, Cambridge (UK), 2006.

[14] D. Cai, J. H. J. Thijssen, and P. S. Clegg. Making non-aqueous high internal phase pickering emulsions: Influence of added polymer and selective drying. *ACS Applied Materials & Interfaces*, 6:9214–9219, 2014.

[15] J. A. Witt, D. R. Mumm, and A. Mohraz. Microstructural tunability of co-continuous bijel-derived electrodes to provide high energy and power densities. *Journal of Materials Chemistry A*, 4:1000–1007, 2016.

[16] U. T. Gonzenbach, A. R. Studart, E. Tervoort, and L. J. Gauckler. Macroporous ceramics from particle-stabilized wet foams. *Journal of the American Ceramic Society*, 90:16–22, 2007.

[17] A. R. Studart, U. T. Gonzenbach, I. Akartuna, E. Tervoort, and L. J. Gauckler. Materials from foams and emulsions stabilized by colloidal particles. *Journal of Materials Chemistry*, 17:3283–3289, 2007.

[18] I. Akartuna, A. R. Studart, E. Tervoort, and L. J. Gauckler. Macroporous ceramics from particle-stabilized emulsions. *Advanced Materials*, 20:4714–4718, 2008.

[19] P. Pieranski. Two-dimensional interfacial colloidal crystals. *Physical Review Letters*, 45:569–572, 1980.

[20] S. Levine, B. D. Bowen, and S. J. Partridge. Stabilization of emulsions by fine particles i. partitioning of particles between continuous phase and oil/water interface. *Colloids and Surfaces*, 38:325–343, 1989.

[21] R. Aveyard, B. P. Binks, and J. H. Clint. Emulsions stabilised solely by colloidal particles. *Advances in Colloid and Interface Science*, 100:503–546, 2003.

[22] V. N. Paunov. Novel method for determining the three-phase contact angle of colloid particles adsorbed at air-water and oil-water interfaces. *Langmuir*, 19:7970–7976, 2003.

[23] A. Goebel and K. Lunkenheimer. Interfacial tension of the water/n-alkane interface. *Langmuir*, 13:369–372, 1997.

[24] D. R. Lide, editor. *CRC Handbook of Chemistry and Physics*. CRC Press, Boca Raton (USA), 2001–2002.

[25] J. Leandri and A. Wurger. Trapping energy of a spherical particle on a curved liquid interface. *Journal of Colloid and Interface Science*, 405:249–255, 2013.

[26] D. Langevin. Influence of interfacial rheology on foam and emulsion properties. *Advances in Colloid and Interface Science*, 88:209–222, 2000.

[27] H. A. Stone, S. A. Koehler, S. Hilgenfeldt, and M. Durand. Perspectives on foam drainage and the influence of interfacial rheology. *Journal of Physics-Condensed Matter*, 15:S283–S290, 2003.

[28] B. S. Murray and P. V. Nelson. A novel langmuir trough for equilibrium and dynamic measurements oil air-water and oil-water monolayers. *Langmuir*, 12:5973–5976, 1996.

[29] M. D. Lacasse, G. S. Grest, D. Levine, T. G. Mason, and D. A. Weitz. Model for the elasticity of compressed emulsions. *Physical Review Letters*, 76:3448–3451, 1996.

[30] L. Maurice, R. A. Maguire, A. B. Schofield, M. E. Cates, P. S. Clegg, and J. H. J. Thijssen. Squeezing particle-stabilized emulsions into biliquid foams - equation of state. *Soft Matter*, 9:7757–7765, 2013.

[31] G. G. Fuller and J. Vermant. Complex fluid-fluid interfaces: Rheology and structure. *Annual Review of Chemical and Biomolecular Engineering*, 3:519–543, 2012.

[32] R. Miller, R. Wustneck, J. Kragel, and G. Kretzschmar. Dilational and shear rheology of adsorption layers at liquid interfaces. *Colloids and Surfaces A-Physicochemical and Engineering Aspects*, 111:75–118, 1996.

[33] S. R. Derkach, J. Kraegel, and R. Miller. Methods of measuring rheological properties of interfacial layers (experimental methods of 2d rheology). *Colloid Journal*, 71:1–17, 2009.

[34] J. Kragel and S. R. Derkatch. Interfacial shear rheology. *Current Opinion in Colloid & Interface Science*, 15:246–255, 2010.

[35] T. Verwijlen, D.L. Leiske, P. Moldenaers, J. Vermant, and G. G. Fuller. Extensional rheometry at interfaces: Analysis of the cambridge interfacial tensiometer. *Journal of Rheology*, 56:1225, 2012.

[36] M. Pepicelli, T. Verwijlen, T. A. Tervoort, and J. Vermant. Characterization and modelling of langmuir interfaces with finite elasticity. *Soft Matter*, 13:5977–5990, 2017.

[37] T. Verwijlen, L. Imperiali, and J. Vermant. Separating viscoelastic and compressibility contributions in pressure-area isotherm measurements. *Advances in Colloid and Interface Science*, 206:428–436, 2014.

[38] P. Erni. Deformation modes of complex fluid interfaces. *Soft Matter*, 7:7586–7600, 2011.

[39] M. Nagel, T. A. Tervoort, and J. Vermant. From drop-shape analysis to stress-fitting elastometry. *Advances in Colloid and Interface Science*, 247:33–51, 2017.

[40] D. Vella, P. Aussillous, and L. Mahadevan. Elasticity of an interfacial particle raft. *Europhysics Letters*, 68:212–218, 2004.

[41] S. Knoche, D. Vella, E. Aumaitre, P. Degen, H. Rehage, P. Cicuta, and J. Kierfeld. Elastometry of

deflated capsules: Elastic moduli from shape and wrinkle analysis. *Langmuir*, 29:12463–12471, 2013.

[42] D. A. Edwards, H Brenner, and D. T. Wasan, editors. *Interfacial Transport Processes and Rheology*. Butterworth-Heinemann, Boston, 1991.

[43] S. Reynaert, C. F. Brooks, P. Moldenaers, J. Vermant, and G. G. Fuller. Analysis of the magnetic rod interfacial stress rheometer. *Journal of Rheology*, 52:261–285, 2008.

[44] S. Barman and G. F. Christopher. Simultaneous interfacial rheology and microstructure measurement of densely aggregated particle laden interfaces using a modified double wall ring interfacial rheometer. *Langmuir*, 30:9752–9760, 2014.

[45] J. B. Segur and H. E. Oberstar. Viscosity of glycerol and its aqueous solutions. *Industrial and Engineering Chemistry*, 43:2117–2120, 1951.

[46] S. Vandebril, A. Franck, G. G. Fuller, P. Moldenaers, and J. Vermant. A double wall-ring geometry for interfacial shear rheometry. *Rheologica Acta*, 49:131–144, 2010.

[47] G. J. Elfring, L. G. Leal, and T. M. Squires. Surface viscosity and marangoni stresses at surfactant laden interfaces. *Journal of Fluid Mechanics*, 792:712–739, 2016.

[48] K. A. Erk, J. D. Martin, J. T. Schwalbe, F. R. Phelan, and S. D. Hudson. Shear and dilational interfacial rheology of surfactant-stabilized droplets. *Journal of Colloid and Interface Science*, 377:442–449, 2012.

[49] T. Verwijlen, P. Moldenaers, and J. Vermant. A fixture for interfacial dilatational rheometry using a rotational rheometer. *The European Physical Journal Special Topics*, 222:83–97, 2013.

[50] A. Maestro, E. Santini, D. Zabiegaj, S. Llamas, F. Ravera, L. Liggieri, F. Ortega, R. G. Rubio, and E. Guzman. Particle and particle-surfactant mixtures at fluid interfaces: Assembly, morphology, and rheological description. *Advances in Condensed Matter Physics*, 2015:917516, 2015.

[51] O. S. Deshmukh, D. van den Ende, M. C. Stuart, F. Mugele, and M. H. G. Duits. Hard and soft colloids at fluid interfaces: Adsorption, interactions, assembly & rheology. *Advances in Colloid and Interface Science*, 222:215–227, 2015.

[52] D. Y. Zang, E. Rio, G. Delon, D. Langevin, B. Wei, and B. P. Binks. Influence of the contact angle of silica nanoparticles at the air-water interface on the mechanical properties of the layers composed of these particles. *Molecular Physics*, 109:1057–1066, 2011.

[53] L. Imperiali, K. H. Liao, C. Clasen, J. Fransaer, C. W. Macosko, and J. Vermant. Interfacial rheology and structure of tiled graphene oxide sheets. *Langmuir*, 28:7990–8000, 2012.

[54] M. Karbaschi, M. Lotfi, J. Kragel, A. Javadi, D. Bastani, and R. Miller. Rheology of interfacial layers. *Current Opinion in Colloid & Interface Science*, 19:514–519, 2014.

[55] R. Van Hooghten, V. E. Blair, A. Vananroye, A. B. Schofield, J. Vermant, and J. H. J. Thijssen. Interfacial rheology of sterically stabilized colloids at liquid interfaces and its effect on the stability of pickering emulsions. *Langmuir*, 33:4107–4118, 2017.

[56] B. P. Binks and S. O. Lumsdon. Catastrophic phase inversion of water-in-oil emulsions stabilized by hydrophobic silica. *Langmuir*, 16:2539–2547, 2000.

[57] B. P. Binks and C. P. Whitby. Nanoparticle silica-stabilised oil-in-water emulsions: improving emulsion stability. *Colloids and Surfaces A-Physicochemical and Engineering Aspects*, 253:105–115, 2005.

[58] L. Imperiali, C. Clasen, J. Fransaer, C. W. Macosko, and J. Vermant. A simple route towards graphene oxide frameworks. *Materials Horizons*, 1:139–145, 2014.

[59] M. E. Cates and P. S. Clegg. Bijels: a new class of soft materials. *Soft Matter*, 4:2132–2138, 2008.

[60] A. Mohraz. Interfacial routes to colloidal gelation. *Current Opinion in Colloid & Interface Science*, 25:89–97, 2016.

[61] J. W. Tavacoli, J. H. J. Thijssen, and P. S. Clegg. Bicontinuous emulsions stabilized by colloidal particles (chapter 6). In *Particle-Stabilized Emulsions and Colloids: Formation and Applications*, pages 129–168. The Royal Society of Chemistry, Cambridge (UK), 2015.

[62] K. Stratford, R. Adhikari, I. Pagonabarraga, J. C. Desplat, and M. E. Cates. Colloidal jamming at interfaces: A route to fluid-bicontinuous gels. *Science*, 309:2198–2201, 2005.

[63] E. M. Herzig, K. A. White, A. B. Schofield, W. C. K. Poon, and P. S. Clegg. Bicontinuous emulsions stabilized solely by colloidal particles. *Nature Materials*, 6:966–971, 2007.

[64] M. N. Lee and A. Mohraz. Bicontinuous macroporous materials from bijel templates. *Advanced Materials*, 22:4836–4841, 2010.

[65] M. Cui, T. Emrick, and T. P. Russell. Stabilizing liquid drops in nonequilibrium shapes by the interfacial jamming of nanoparticles. *Science*, 342:460–463, 2013.

[66] M. F. Haase, K. J. Stebe, and D. Lee. Continuous fabrication of hierarchical and asymmetric bijel microparticles, fibers, and membranes by solvent transfer-induced phase separation (strips). *Advanced Materials*, 27:7065–7071, 2015.

[67] D. Cai, P. S. Clegg, T. Li, K. A. Rumble, and J. W. Tavacoli. Bijels formed by direct mixing. *Soft Matter*, 13:4824–4829, 2017.

[68] Fabian Jansen and Jens Harting. From bijels to pickering emulsions: A lattice boltzmann study. *Physical Review E*, 83:046707, 2011.

[69] Kathryn A. White, Andrew B. Schofield, Philip Wormald, Joseph W. Tavacoli, Bernard P. Binks, and Paul S. Clegg. Inversion of particle-stabilized emulsions of partially miscible liquids by mild drying of modified silica particles. *Journal of Colloid and Interface Science*, 359:126–135, 2011.

[70] J. W. Tavacoli, J. H. J. Thijssen, A. B. Schofield, and P. S. Clegg. Novel, robust, and versatile bijels of nitromethane, ethanediol, and colloidal silica: Capsules, sub-ten-micrometer domains, and mechanical properties. *Advanced Functional Materials*, 21:2020–2027, 2011.

[71] Thomson Reuters. Web of science. `https://apps.webofknowledge.com/`. Accessed: 2017-01-01.

[72] M. Reeves, A. T. Brown, A. B. Schofield, M. E. Cates, and J. H. J. Thijssen. Particle-size effects in the formation of bicontinuous pickering emulsions. *Physical Review E*, 92:032308, 2015.

[73] N. Tanaka, H. Kobayashi, N. Ishizuka, H. Minakuchi, K. Nakanishi, K. Hosoya, and T. Ikegami. Monolithic silica columns for high-efficiency chromatographic separations. *Journal of Chromatography A*, 965:35–49, 2002.

[74] I. K. Sung, Christian, M. Mitchell, D. P. Kim, and P. J. A. Kenis. Tailored macroporous sicn and sic structures for high-temperature fuel reforming. *Advanced Functional Materials*, 15:1336–1342, 2005.

[75] M. Martina, G. Subramanyam, J. C. Weaver, D. W. Hutmacher, D. E. Morse, and S. Valiyaveettil. Developing macroporous bicontinuous materials as scaffolds for tissue engineering. *Biomaterials*, 26:5609–5616, 2005.

[76] J. A. Witt, D. R. Mumm, and A. Mohraz. Bijel reinforcement by droplet bridging: a route to bicontinuous materials with large domains. *Soft Matter*, 9:6773–6780, 2013.

[77] M. N. Lee, J. H. J. Thijssen, J. A. Witt, P. S. Clegg, and A. Mohraz. Making a robust interfacial scaffold: Bijel rheology and its link to processability. *Advanced Functional Materials*, 23:417–423, 2013.

[78] M. F. Haase, N. Sharifi-Mood, D. Lee, and K. J. Stebe. In situ mechanical testing of nanostructured bijel fibers. *ACS Nano*, 10:6338–6344, 2016.

[79] K. A. Rumble, J. H. J. Thijssen, A. B. Schofield, and P. S. Clegg. Compressing a spinodal surface at fixed area: bijels in a centrifuge. *Soft Matter*, 12:4375–4383, 2016.

[80] L. Bai, J. W. Fruehwirth, X. Cheng, and C. W. Macosko. Dynamics and rheology of nonpolar bijels. *Soft Matter*, 11:5282–5293, 2015.

[81] P. A. Kralchevsky, V. N. Paunov, I. B. Ivanov, and K. Nagayama. Capillary meniscus interaction between colloidal particles attached to a liquid-fluid interface. *Journal of Colloid and Interface Science*, 151:79–94, 1992.

[82] P. A. Kralchevsky, V. N. Paunov, N. D. Denkov, I. B. Ivanov, and K. Nagayama. Energetical and force approaches to the capillary interactions between particles attached to a liquid fluid

interface. *Journal of Colloid and Interface Science*, 155:420–437, 1993.

[83] S. Arditty, V. Schmitt, F. Lequeux, and F. Leal-Calderon. Interfacial properties in solid-stabilized emulsions. *European Physical Journal B*, 44:381–393, 2005.

[84] J. W. O. Salari, F. A. M. Leermakers, and B. Klumperman. Pickering emulsions: Wetting and colloidal stability of hairy particles-a self-consistent field theory. *Langmuir*, 27:6574–6583, 2011.

[85] W. B. Russel, D. A. Saville, and W. R. Schowalter. *Colloidal Dispersions*. Cambridge University Press, Cambridge (UK), 1999.

[86] H. Firoozmand and D. Rousseau. Microbial cells as colloidal particles: Pickering oil-in-water emulsions stabilized by bacteria and yeast. *Food Research International*, 81:66–73, 2016.

[87] J. D. Wu, M. X. Shi, W. Li, L. H. Zhao, Z. Wang, X. Z. Yan, W. Norde, and Y. Li. Pickering emulsions stabilized by whey protein nanoparticles prepared by thermal cross-linking. *Colloids and Surfaces B-Biointerfaces*, 127:96–104, 2015.

[88] Y. M. Feng and Y. Lee. Surface modification of zein colloidal particles with sodium caseinate to stabilize oil-in-water pickering emulsion. *Food Hydrocolloids*, 56:292–302, 2016.

[89] M. Rayner, D. Marku, M. Eriksson, M. Sjoo, P. Dejmek, and M. Wahlgren. Biomass-based particles for the formulation of pickering type emulsions in food and topical applications. *Colloids and Surfaces A-Physicochemical and Engineering Aspects*, 458:48–62, 2014.

[90] J. Xiao, Y. Q. Li, and Q. R. Huang. Recent advances on food-grade particles stabilized pickering emulsions: Fabrication, characterization and research trends. *Trends in Food Science & Technology*, 55:48–60, 2016.

[91] S. Lam, K. P. Velikov, and O. D. Velev. Pickering stabilization of foams and emulsions with particles of biological origin. *Current Opinion in Colloid & Interface Science*, 19:490–500, 2014.

[92] Y. Q. Yang, Z. W. Fang, X. Chen, W. W. Zhang, Y. M. Xie, Y. H. Chen, Z. G. Liu, and W. E. Yuan. An overview of pickering emulsions: Solid-particle materials, classification, morphology, and applications. *Frontiers in Pharmacology*, 8:287, 2017.

[93] S. M. Zhang, Y. H. Zhou, and C. Yang. Pickering emulsions stabilized by the complex of polystyrene particles and chitosan. *Colloids and Surfaces A-Physicochemical and Engineering Aspects*, 482:338–344, 2015.

[94] ThermoFisher Scientific. Idc surfactant-free latex beads. `https://www.thermofisher.com/uk/en/home/life-science/cell-analysis/qdots-microspheres-nanospheres/idc-surfactant-free-latex-beads.html`. Accessed: 2016-03-15.

[95] J. H. Prescott, S. J. Shiau, and R. L. Rowell. Characterization of polystyrene latexes by hydrodynamic and electrophoretic fingerprinting. *Langmuir*, 9:2071–2076, 1993.

[96] G. K. Min, M. A. Bevan, D. C. Prieve, and G. D. Patterson. Light scattering characterization of polystyrene latex with and without adsorbed polymer. *Colloids and Surfaces A-Physicochemical and Engineering Aspects*, 202:9–21, 2002.

[97] D. E. Dunstan and J. Stokes. Diffusing probe measurements of polystyrene latex particles in polyelectrolyte solutions: Deviations from stokes-einstein behavior. *Macromolecules*, 33:193–198, 2000.

[98] R. L. Xu. Shear plane and hydrodynamic diameter of microspheres in suspension. *Langmuir*, 14:2593–2597, 1998.

[99] M. R. Gittings and D. A. Saville. The determination of hydrodynamic size and zeta potential from electrophoretic mobility and light scattering measurements. *Colloids and Surfaces A-Physicochemical and Engineering Aspects*, 141:111–117, 1998.

[100] J. D. Feick and D. Velegol. Measurements of charge nonuniformity on polystyrene latex particles. *Langmuir*, 18:3454–3458, 2002.

[101] L. Isa, F. Lucas, R. Wepf, and E. Reimhult. Measuring single-nanoparticle wetting properties by freeze-fracture shadow-casting cryo-scanning electron microscopy. *Nature Communications*, 2:438, 2011.

[102] I. Popa and F. Marlow. Post-deposition opal evolution. *Chemphyschem*, 9:1541–1547, 2008.

[103] M. A. Agam and Q. Guo. Electron beam modification of polymer nanospheres. *Journal of Nanoscience and Nanotechnology*, 7:3615–3619, 2007.

[104] L. Farias-Cepeda, J. Herrera-Ordonez, and E. Saldivar-Guerra. Effect of surfactant on the swelling of polymeric nanoparticles: toward a generalized approach. *Colloid and Polymer Science*, 287:1215–1220, 2009.

[105] P. A. Kralchevsky and K. Nagayama. Capillary interactions between particles bound to interfaces, liquid films and biomembranes. *Advances in Colloid and Interface Science*, 85:145–192, 2000.

[106] D. Vella. Floating versus sinking. *Annual Review of Fluid Mechanics*, 47:115–35, 2015.

[107] R. M. Fitch. *Polymer Colloids: A Comprehensive Introduction*. Academic Press, London, 1997.

[108] B. J. Park, J. Vermant, and E. M. Furst. Heterogeneity of the electrostatic repulsion between colloids at the oil-water interface. *Soft Matter*, 6:5327–5333, 2010.

[109] S. Reynaert, P. Moldenaers, and J. Vermant. Control over colloidal aggregation in monolayers of latex particles at the oil-water interface. *Langmuir*, 22:4936–4945, 2006.

[110] S. Coertjens, P. Moldenaers, J. Vermant, and L. Isa. Contact angles of microellipsoids at fluid interfaces. *Langmuir*, 30:4289–4300, 2014.

[111] D. M. Kaz, R. McGorty, M. Mani, M. P. Brenner, and V. N. Manoharan. Physical ageing of the contact line on colloidal particles at liquid interfaces. *Nature materials*, 11:138–142, 2012.

[112] A. Wang, R. McGorty, D. M. Kaz, and V. N. Manoharan. Contact-line pinning controls how quickly colloidal particles equilibrate with liquid interfaces. *Soft matter*, 12:8958–8967, 2016.

[113] I. T. Horvath, P. Colinet, and M. R. Vetrano. Measuring contact angles of small spherical particles at planar fluid interfaces by light extinction. *Applied Physics Letters*, 108:201605, 2016.

[114] J. H. Brooks and B. A. Pethica. Properties of ionized monolayers .6. film pressures of ionized spread monalayers at heptane/water interface. *Transactions of the Faraday Society*, 60:208–215, 1964.

[115] J. D. Berry, M. J. Neeson, R. R. Dagastine, D. Y. C. Chan, and R. F. Tabor. Measurement of surface and interfacial tension using pendant drop tensiometry. *Journal of Colloid and Interface Science*, 454:226–237, 2015.

[116] G. G. Fuller and J. Vermant. Editorial: dynamics and rheology of complex fluid-fluid interfaces. *Soft Matter*, 7:7583–7585, 2011.

[117] Alma J. Mendoza, Eduardo Guzman, Fernando Martinez-Pedrero, Hernan Ritacco, Ramon G. Rubio, Francisco Ortega, Victor M. Starov, and Reinhard Miller. Particle laden fluid interfaces: Dynamics and interfacial rheology. *Advances in Colloid and Interface Science*, 206:303–319, 2014.

[118] M. Reeves, K. Stratford, and J. H. J. Thijssen. Quantitative morphological characterization of bicontinuous pickering emulsions via interfacial curvatures. *Soft Matter*, 12:4082–4092, 2016.

[119] R. Aveyard, J. H. Clint, D. Nees, and V. N. Paunov. Compression and structure of monolayers of charged latex particles at air/water and octane/water interfaces. *Langmuir*, 16:1969–1979, 2000.

[120] R. Aveyard, B. P. Binks, J. H. Clint, P. D. I. Fletcher, T. S. Horozov, B. Neumann, V. N. Paunov, J. Annesley, S. W. Botchway, D. Nees, A. W. Parker, A. D. Ward, and A. N. Burgess. Measurement of long-range repulsive forces between charged particles at an oil-water interface. *Physical Review Letters*, 88:246102, 2002.

[121] J. Z. Sun and T. Stirner. Molecular dynamics simulation of the surface pressure of colloidal monolayers. *Langmuir*, 17:3103–3108, 2001.

[122] P. Gao, X. Xing, Y. Li, T. Ngai, and F. Jin. Charging and discharging of single colloidal particles at oil/water interfaces. *Scientific Reports*, 4:4778, 2014.

[123] B. J. Park, J. P. Pantina, E. M. Furst, M. Oettel, S. Reynaert, and J. Vermant. Direct measurements of the effects of salt and surfactant on interaction forces between colloidal particles at water-oil interfaces. *Langmuir*, 24:1686–1694, 2008.

[124] K. Masschaele, B. J. Park, E. M. Furst, J. Fransaer, and J. Vermant. Finite ion-size effects dominate the interaction between charged colloidal particles at an oil-water interface. *Physical*

Review Letters, 105:048303, 2010.

[125] D. Frydel and M. Oettel. Charged particles at fluid interfaces as a probe into structural details of a double layer. *Physical Chemistry Chemical Physics*, 13:4109–4118, 2011.

[126] C. L. Wirth, E. M. Furst, and J. Vermant. Weak electrolyte dependence in the repulsion of colloids at an oil–water interface. *Langmuir*, 30:2670–2675, 2014.

[127] R. Aveyard, J. H. Clint, D. Nees, N. Quirke, and Ay. Structure and collapse of particle monolayers under lateral pressure at the octane/aqueous surfactant solution interface. *Langmuir*, 16:8820–8828, 2000.

[128] V. Garbin, J. C. Crocker, and K. J. Stebe. Forced desorption of nanoparticles from an oil-water interface. *Langmuir*, 28:1663–1667, 2012.

[129] N. I. D. Fenwick, F. Bresme, and N. Quirke. Computer simulation of a langmuir trough experiment carried out on a nanoparticulate array. *Journal of Chemical Physics*, 114:7274–7282, 2001.

[130] J. Israelachvili. *Intermolecular and Surface Forces*. Academic, San Diego, 1998.

[131] A. R. Cox, B. Vincent, S. Harley, and S. E. Taylor. Characterisation of spread monolayers of functionalised polyisobutylenes with various chain architectures. *Colloids and Surfaces A-Physicochemical and Engineering Aspects*, 146:153–162, 1999.

[132] J. W. Tavacoli, G. Katgert, E. G. Kim, M. E. Cates, and P. S. Clegg. Size limit for particle-stabilized emulsion droplets under gravity. *Physical Review Letters*, 108:268306, 2012.

[133] M. S. Manga, T. N. Hunter, O. J. Cayre, D. W. York, M. D. Reichert, S. L. Anna, L. M. Walker, R. A. Williams, and S. R. Biggs. Measurements of submicron particle adsorption and particle film elasticity at oil-water interfaces. *Langmuir*, 32:4125–4133, 2016.

[134] C. Gu and L. Botto. Direct calculation of anisotropic surface stresses during deformation of a particle-covered drop. *Soft Matter*, 12:705–716, 2016.

[135] E. J. W. Verwey and J. Th. G. Overbeek. *Theory of the stability of lyophobic colloids*. Dover Publications, Inc., Mineola (New York), 1999.

[136] J. S. Rowlinson and B. Widom. *Molecular theory of capillarity*. Dover Publications, Inc., Mineola (New York), 2013.

[137] S. Reynaert, P. Moldenaers, and J. Vermant. Interfacial rheology of stable and weakly aggregated two-dimensional suspensions. *Physical Chemistry Chemical Physics*, 9:6463–6475, 2007.

[138] K. D. Danov, R. D. Stanimirova, P. A. Kralchevsky, K. G. Marinova, N. A. Alexandrov, S. D. Stoyanov, T. B. J. Blijdenstein, and E. G. Pelan. Capillary meniscus dynamometry - method for determining the surface tension of drops and bubbles with isotropic and anisotropic surface stress distributions. *Journal of Colloid and Interface Science*, 440:168–178, 2015.

[139] E. J. Stancik, A. L. Hawkinson, J. Vermant, and G. G. Fuller. Dynamic transitions and oscillatory melting of a two-dimensional crystal subjected to shear flow. *Journal of Rheology*, 48:159–173, 2004.

[140] K. Masschaele, J. Fransaer, and J. Vermant. Direct visualization of yielding in model two-dimensional colloidal gels subjected to shear flow. *Journal of Rheology*, 53:1437–1460, 2009.

[141] S. M. Fielding. Complex dynamics of shear banded flows. *Soft Matter*, 3:1262–1279, 2007.

[142] T. S. Horozov and B. P. Binks. Particle behaviour at horizontal and vertical fluid interfaces. *Colloids and Surfaces A-Physicochemical and Engineering Aspects*, 267:64–73, 2005.

[143] A. D. Law, D. M. A. Buzza, and T. S. Horozov. Two-dimensional colloidal alloys. *Physical Review Letters*, 106:128302, 2011.

[144] S. Barman and G. F. Christopher. Role of capillarity and microstructure on interfacial viscoelasticity of particle laden interfaces. *Journal of Rheology*, 60:35–45, 2016.

[145] S. Biswas, M. Grant, I. Samajdar, A. Haldar, and A. Sain. Micromechanics of emergent patterns in plastic flows. *Scientific Reports*, 3:2728, 2013.

[146] N. C. Keim and P. E. Arratia. Yielding and microstructure in a 2d jammed material under shear deformation. *Soft Matter*, 9:6222–6225, 2013.

[147] I. Buttinoni, Z. A. Zell, T. M. Squires, and L. Isa. Colloidal binary mixtures at fluid-fluid

interfaces under steady shear: structural, dynamical and mechanical response. *Soft Matter*, 11:8313–8321, 2015.

[148] I. Buttinoni, M. Steinacher, H. Th. Spanke, J. Pokki, S. Bahmann, B. Nelson, G. Foffi, and L. Isa. Colloidal polycrystalline monolayers under oscillatory shear. *Physical Review E*, 95:012610, 2017.

[149] T.D. Kassuga and J. P. Rothstein. Buckling of particle-laden interfaces. *Journal of Colloid and Interface Science*, 448:287–296, 2015.

[150] P. A. Kralchevsky, I. B. Ivanov, K. P. Ananthapadmanabhan, and A. Lips. On the thermodynamics of particle-stabilized emulsions: Curvature effects and catastrophic phase inversion. *Langmuir*, 21:50–63, 2005.

[151] J. Lucassen. Dynamic dilational properties of composite surfaces. *Colloids and Surfaces*, 65:139–149, 1992.

[152] L. D. Landau and E. M. Lifschitz. *Theory of Elasticity*. Pergamon, Oxford, 1970.

[153] C. Planchette, E. Lorenceau, and A.-L. Biance. Surface wave on a particle raft. *Soft Matter*, 8:2444–2451, 2012.

[154] R. Aveyard, J. H. Clint, and T. S. Horozov. Aspects of the stabilisation of emulsions by solid particles: Effects of line tension and monolayer curvature energy. *Physical Chemistry Chemical Physics*, 5:2398–2409, 2003.

[155] S. Arditty, C. P. Whitby, B. P. Binks, V. Schmitt, and F. Leal-Calderon. Some general features of limited coalescence in solid-stabilized emulsions. *European Physical Journal E*, 11:273–281, 2003.

[156] B. Madivala, S. Vandebril, J. Fransaer, and J. Vermant. Exploiting particle shape in solid stabilized emulsions. *Soft Matter*, 5:1717–1727, 2009.

[157] S. Arditty, V. Schmitt, J. Giermanska-Kahn, and F. Leal-Calderon. Materials based on solid-stabilized emulsions. *Journal of Colloid and Interface Science*, 275:659–664, 2004.

[158] A. B. Pawar, M. Caggioni, R. Ergun, R. W. Hartel, and P. T. Spicer. Arrested coalescence in pickering emulsions. *Soft Matter*, 7:7710–7716, 2011.

[159] Bernard P. Binks and Ryo Murakami. Phase inversion of particle-stabilized materials from foams to dry water. *Nature Materials*, 5:865–869, 2006.

[160] A. B. Subramaniam, M. Abkarian, L. Mahadevan, and H. A. Stone. Non-spherical bubbles. *Nature*, 438:930–930, 2005.

[161] T. Wu, H. T. Wang, B. X. Jing, F. Liu, P. C. Burns, and C. Z. Na. Multi-body coalescence in pickering emulsions. *Nature Communications*, 6:5929, 2015.

[162] D. E. Tambe and M. M. Sharma. The effect of colloidal particles on fluid-fluid interfacial properties and emulsion stability. *Advances in Colloid and Interface Science*, 52:1–63, 1994.

[163] M. N. Lee, H. K. Chan, and A. Mohraz. Characteristics of pickering emulsion gels formed by droplet bridging. *Langmuir*, 28:3085–3091, 2012.

[164] T.-L. Cheng and Y. U. Wang. Shape-anisotropic particles at curved fluid interfaces and role of laplace pressure: A computational study. *Journal of Colloid and Interface Science*, 402:267–278, 2013.

[165] S. Aland, J. Lowengrub, and A. Voigt. A continuum model of colloid-stabilized interfaces. *Physics of Fluids*, 23:062103, 2011.

[166] S. Aland, J. Lowengrub, and A. Voigt. Particles at fluid-fluid interfaces: A new navier-stokes-cahn-hilliard surface-phase-field-crystal model. *Physical Review E*, 86:046321, 2012.

[167] R. G. M. van der Sman and M. B. J. Meinders. Mesoscale models of dispersions stabilized by surfactants and colloids. *Advances in Colloid and Interface Science*, 211:63–76, 2014.

[168] J. R. Samaniuk and J. Vermant. Micro and macrorheology at fluid-fluid interfaces. *Soft Matter*, 10:7023–7033, 2014.